ERK1/2 is an ancestral organising signal in spiral cleavage

Océane Seudre[1,2], Allan M. Carrillo-Baltodano[1,2], Yan Liang[1], José M. Martín-Durán[1*]

[1] School of Biological and Chemical Sciences. Queen Mary University of London. Mile End Road, E1 4NS, London. United Kingdom.

[2] These authors contributed equally to this work.

[*]Correspondence: chema.martin@qmul.ac.uk

SUMMARY

Embryonic organisers are signalling centres that instruct the establishment of body plans during animal embryogenesis, thus underpinning animal morphological diversity. In spiral cleavage – a stereotypic developmental programme ancestral to 14, nearly half, of the major animal groups (e.g., molluscs, annelids and flatworms), a cell known as the D-quadrant organiser defines cell fates and the body axes. ERK1/2 specifies the embryonic organiser in molluscs, yet how this signalling cascade exerts organising activity and whether this role is conserved in other spiral cleaving groups is unclear. Here, we demonstrate that ERK1/2 promotes the specification and inductive activity of the D-quadrant organiser in *Owenia fusiformis*, an early-branching annelid exhibiting ancestral developmental traits. In this species, active di-phosphorylated ERK1/2 mediated by FGF receptor activity localises to the 4d micromere, establishing the bilateral symmetry and specifying the hindgut and trunk mesodermal progenitor. Accordingly, impairing FGFR and ERK1/2 activity, as well as cell communication results in embryos developing anteroventrally radialised. Differential

transcriptomic profiling shows the ParaHox *cdx* and the Notch ligand *delta* as FGFR/ERK1/2 downstream targets in 4d, further revealing that 4d specification instructs the expression of mesodermal and posterodorsal genes in neighbouring cells, putatively via the Notch pathway. The instructing role of ERK1/2 in the D-quadrant organiser is thus shared between *O. fusiformis* and molluscs, representing an ancestral trait of spiral cleavage. Altogether, our study begins to dissect the gene network promoting axial patterning and posterior growth in spiral cleavage, revealing extensive mechanistic diversification in body plan specification despite overall conservation of cleavage patterns in Spiralia.

Keywords: spiral cleavage, Spiralia, embryonic organiser, D-quadrant organiser, annelid, ERK1/2, MAPK pathway, FGF pathway, Notch pathway.

Introduction

Embryonic organisers are cells or groups of cells able to instruct neighbouring tissues towards certain fates and behaviours during animal embryogenesis [1, 2] (Figure 1A). Embryonic organisers thus play a critical role in patterning tissues and organs, promoting morphogenetic processes that establish animal body plans, thereby emerging as potential drivers of morphological evolution [3-5]. Spiralia is a clade of bilaterally symmetrical animals (Bilateria) comprising nearly half of the major animal clades, including morphologically disparate groups such as molluscs, flatworms and annelids [6, 7]. A stereotypic early developmental programme termed spiral cleavage, characterised by alternating clockwise and counterclockwise oblique cell divisions from the 4-cell stage onwards [8, 9] is however widespread, and likely ancestral to Spiralia [8, 10, 11] (Figure 1A). How spiral cleavage generates the vast diversity of spiralian body plans is still unclear (Figure 1A), albeit this being fundamental to understand the evolution of animal development and morphology.

Spiral cleavage involves the formation of an embryonic organiser that instructs cell fates around four embryonic quadrants, named A to D, which roughly correspond to the left, ventral, right and dorsal sides of the embryo respectively [8, 9]. It is a cell belonging to the D-quadrant – e.g., the 3D or 4d blastomeres in molluscs [12] – that acts as embryonic organiser, and thus this signalling centre is named D-quadrant organiser (Figure 1A). The most common and probably ancestral mode to specify the D-quadrant and its organising cell is through inductive signals at around the 32-cell stage [13, 14]. This type of spiral cleavage is termed conditional; or equal, since early embryos exhibit quadri-radial symmetry during early stages. However, in some mollusc and annelid species, the specification of the D-quadrant organiser is largely cell-autonomous, as two asymmetric zygotic divisions segregate maternal mRNAs to one (the D) blastomere at the 4-cell stage [9, 13, 14]. This autonomous mode of spiral

cleavage is also referred to as unequal, because the D founder cell at the 4-cell stage is larger. Regardless of the specification mode, the ERK1/2 signalling pathway, an evolutionarily conserved intracellular cascade of kinases involved in an array of cellular processes [15], is active and necessary in the D-quadrant organiser in molluscs [16-20] (Table S1). However, what activates ERK1/2 and how ERK1/2 orchestrates the instructing role of the D-quadrant organiser in this group is not understood (Figure 1A), and thus how embryonic organisers define the spiralian body plan is still an unresolved question.

The role of ERK1/2 signalling during spiral cleavage in groups other than Mollusca is in addition ambiguous and only explored in Annelida (Table S1). As in molluscs, the conditional cleaving annelid *Hydroides hexagonus* exhibits active ERK1/2 in the 4d cell [17], which is often called “mesentoblast” and cell lineage analyses identify as the trunk mesodermal precursor in most annelid embryos [21-23]. Yet the role of ERK1/2 in the 4d cell of *H. hexagonus* is unknown. In autonomous cleaving annelids, the patterns of ERK1/2 activity differ markedly between species (Table S1), but in general ERK1/2 is not active in 4d and its inhibition does not result in axial polarity defects in any of the studied species [24-27]. Indeed, the organiser activity occurs in the 2d blastomere and $2d^{11}$ + 4d in the autonomous cleaving annelids *Capitella teleta* and *Tubifex tubifex* respectively [26, 28]; and its inductive role relies on Activin/Nodal activity, and not on ERK1/2 signalling in the autonomous species *C. teleta* and *Chaetopterus pergamentaceus* [24, 29]. Therefore, the cellular and molecular basis underpinning D-quadrant organiser specification and activity varies considerably within Annelida, which ultimately prevents inferring whether ERK1/2 activity in the D-quadrant organiser is a homologous trait to Spiralia or a molluscan innovation that also appeared convergently in some annelid lineages.

The annelid worm *Owenia fusiformis* belongs to Palaeoannelida – the sister group to all remaining annelids [30] – and exhibits embryonic traits considered ancestral to Annelida, including conditional spiral cleavage, formation of a coeloblastula, gastrulation by invagination and the development of a planktotrophic trochophore-like larva [31] (Figure 1B, C). While inductive signals appear to control the establishment of the axial polarity in *O. fusiformis* [32], which blastomere acts as D-quadrant organiser and how this signalling centre becomes specified and controls body patterning is unknown. Therefore, investigating the nature of the D-quadrant organiser and the role of the ERK1/2 signalling pathway in *O. fusiformis* can, by comparison with other annelid and molluscan lineages, help to infer ancestral character states to Annelida and Spiralia as a whole, ultimately contributing to our understanding of the evolution of spiral cleavage and spiralian body plans.

Results

Di-phosphorylated ERK1/2 is enriched in the 4d cell in O. fusiformis

The annelid *O. fusiformi*s has a single ERK1/2 ortholog (Figure S1A), which is expressed at low levels in active oocytes (Figure S1B). The expression of *erk1/2* is stable during early cleavage divisions and up to 4 hours post fertilisation (hpf; ~32 cell stage), increasing thereafter and plateauing at the larval stage (Figure S1B). A cross-reactive antibody against the active di-phosphorylated form of ERK1/2 (di-P-ERK1/2) [16, 17] shows weak ubiquitous signal in the zygote and up to 3 hpf (~16 cell stage) (Figure S1C). At 4 hpf, however, the four most animal/apical micromeres ($1q^{111}$) exhibit enriched di-P-ERK1/2 signal, which disappears at 5 hpf (coeloblastula) (Figure 1D, Figure S1C). At this stage, a single cell in the vegetal pole, which positionally corresponds to a fourth quartet micromere (4q), shows strong signal for di-P-ERK1/2 (Figure 1D, Figure S1C). In *O. fusiformis*, the fourth micromere quartet (4q) starts to form at 4 hpf, when the 3Q macromeres sharing the vegetal cross furrow divide

(Figure 1E). This creates an asymmetry in the timing and order of appearance of the 4q micromeres that is also observed during cleavage of the 3q micromeres, which divide in a counterclockwise order after all 3Q macromeres have cleaved (Figure 1E). By 5 hpf however, the vegetal pole exhibits again a symmetrical arrangement (Figure 1E). At 6 hpf, with the onset of gastrulation [31], di-P-ERK1/2 signal is enriched in seven vegetal cells forming a bilaterally symmetrical pattern that includes one 4q micromere and the $2q^{12}$ and $2q^{22}$ blastomeres of the other three embryonic quadrants (Figure 1D, Figure S1C). At this stage, the 4Q macromeres have cleaved synchronously into the 5Q and 5q cells and all but the 4q micromere enriched in di-P-ERK1/2 have divided, becoming the earliest morphological sign of bilateral symmetry in *O. fusiformis* embryos. This di-P-ERK1/2 positive 4q micromere divides into two large cells only after ingression during early gastrulation at 7 hpf (Figure 1E), with the later progeny occupying a bilateral position on the posterodorsal side of the archenteron once gastrulation completes at 9 hpf (Figure 1E). The behaviour of this 4q micromere resembles the cellular dynamics described for the 4d micromere in other conditional spiral cleaving annelids [33-36], suggesting that the di-P-ERK1/2 enriched 4q micromere at 5 and 6 hpf is the 4d cell and its two large daughter cells are the MR/ML mesoteloblasts (Figure 1D, E). Therefore, ERK1/2 signalling activates first in the $1q^{111}$ animal micromeres and subsequently in the 4d micromere in the annelid *O. fusiformis*, which is similar to the spatiotemporal dynamics of ERK1/2 activity reported in spiral cleaving molluscs (Table S1).

***ERK1/2 signalling controls axial polarity in* O. fusiformis**

To examine the role of the ERK1/2 signalling during *O. fusiformis* development, we treated embryos with brefeldin A (BFA), an inhibitor of intracellular protein trafficking previously used to block the induction of the organiser in other spiral cleaving embryos [32, 37], and

U0126, a selective inhibitor of MEK1/2 and ERK1/2 di-phosphorylation [16, 38] (Figure 2A). For both drugs, treatment from fertilisation (~0.5 hpf) to 5 hpf, when di-P-ERK1/2 is enriched in 4d, effectively blocks activation of ERK1/2 (Figure 2B; Figures S2A; Table S2) and causes the loss of bilateral symmetry, posterior structures (e.g., chaetae and hindgut) and larval muscles in 100% of the embryos at a 10 µM concentration (Figure 2C; Figure S2B; Table S3, S4). Compared to control samples, 0.5 to 5 hpf treated embryos lack a fully formed apical tuft and apical organ, showing reduced ectodermal expression of the apical organ marker *six3/6* [39] and just a few apical cells positive for the neuronal marker *synaptotagmin-1* (*syt-1*) [31] (Figure 2D). In addition, treated embryos lack expression of hindgut (*cdx*) and trunk mesodermal (*twist*) markers [39], exhibit expanded expression of the oral ectodermal marker gene *gsc* [39] around the single gut opening (Figure 2D; Figure S2C), and retain expression of the midgut endodermal marker *GATA4/5/6b* [39] (Figure S2C). We deem this phenotype as antero-ventrally radialised (or Radial; Figure 2C, E). Therefore, activation of ERK1/2 signalling in the 4d cell at the coeloblastula stage relies on inductive cell-cell communication signals (impaired by BFA treatment) required to specify and develop posterior and dorsal structures during *O. fusiformis* embryogenesis.

To dissect the exact timing of induction and activity of ERK1/2 during *O. fusiformis* cleavage, we treated embryos with 10µM BFA/U0126 in overlapping time windows from fertilisation to early gastrulation (Figure 2E; Table S5). Blocking protein secretion with BFA from fertilisation to the 8-cell stage does not affect normal development. However, BFA treatment between the 8-cell stage and 4 hpf results in larvae with all morphological landmarks of a typical mitraria larva and normal expression of tissue-specific markers, but with a compressed morphology (Figure 2F; Figure S2C). Only treatment with BFA from 4 hpf to 6 hpf, and hence spanning the formation of 4d, causes a radial phenotype, with treatments after 5 hpf

being lethal (Figure 2E, Figure S2C). This suggests that the intercellular communication event inducing the activation of ERK1/2 in 4d happens between 4 and 5 hpf, right during 4q micromere formation (Figure 1E). Unexpectedly, preventing ERK1/2 di-phosphorylation with U0126 from the 2-cell stage until 4 hpf, when this induction event might begin, also causes a radial phenotype (Figure 2E), with just slight differences between certain timepoints; embryos treated between 2-cells and 3 hpf show expression of the mesodermal marker *twist* in a few discrete cells, and embryos treated from 4 to 6 hpf are seemingly more elongated along the apical-oral axis (Figure S2C). Therefore, ERK1/2 activity is essential for normal embryonic patterning and posterodorsal development throughout most spiral cleavage in *O. fusiformis*. However, the combination of BFA and U0126 phenotypes suggest that ERK1/2 acts autonomously from the 2-cell stage to 4 hpf, while it requires of inductive cell-to-cell communication signals for its enrichment in 4d.

ERK1/2 signalling activates posterodorsal and mesodermal genes

To investigate the mechanisms through which ERK1/2 controls posterodorsal development in *O. fusiformis*, we hypothesised that genome-wide profiling of gene expression in BFA and U0126 treated embryos would uncover upstream regulators and downstream targets of ERK1/2 activity. We thus treated embryos with either 10 µM BFA or 10 µM U0126 from fertilisation to 5 hpf (to cover both the autonomous and conditional phases of ERK1/2 activity) and performed RNA-seq transcriptome profiling in treated and controlled embryos collected right after di-P-ERK1/2 enrichment in the 4d cell (coeloblastula; 5.5 hpf) and at the larval stage (Figure 3A). Principal component analysis (PCA) and sample-to-sample distance matrices clustered transcriptomic profiles according to developmental stage and biological replica (Figure S3A, B). Differential expression analyses revealed 90 and 268 differentially expressed genes (DEGs; Log Fold Change < -1.5 and adjusted p-value < 0.05) in BFA treated

coeloblastula and larva respectively, and 132 (coeloblastula) and 373 (larva) DEGs after U0126 treatment (Figure 3B). When considering all comparisons and removing redundancies, we detected a total of 628 DEGs, 414 (65.92%) of which were functionally annotated and enriched in gene ontology terms related to regulation of transcription, development and cell fate specification (Table S6, S7, S8). Most of these DEGs were downregulated (Figure 3B, C; Figure S3C, D), with 26 genes downregulated under both drug treatments at the coeloblastula stage and 154 genes commonly downregulated at the larval stage. Only three DEGs (*cdx*, *fer3* and *foxH*) appeared systematically downregulated in both drugs and in the two developmental time points, while we did not identify any common upregulated DEG (Figure 3B; Figure S3D). Therefore, our approach revealed a confident and relatively small set of genes whose expression is dependent on ERK1/2 activity and early inductive signals in *O. fusiformis* embryos.

To validate the set of genes affected by 4d misspecification, we selected 22 candidate genes for further gene expression analyses (Figure 3D, Table S9), including a variety of transcription factors recurrently involved in axial embryonic patterning (e.g., *six3/6*, *gsc*, *cdx*, *AP2*, *foxQ2*), mesoderm development (e.g., *twist*, *hand2*, *foxH*) and neurogenesis (e.g., *POU4*, *irxA*), Wnt ligands (*wnt1*, *wntA* and *wnt4)*, TGF-β modulators (*noggin* and *BAMBI*), and Notch signalling components (*delta* and *notch-like*) (Table S8). Stage-specific RNA-seq data covering twelve developmental time-points, from the unfertilized oocyte to the mature larva, confirmed that for all candidate genes, their expression upregulates at the time of or just after 4d specification and di-P-ERK1/2 enrichment in this cell (Figure 3D). These genes are expressed either in apical/anterior domains (*noggin*, *BAMBI*, *foxQ2*, *POU4*, *six3/6*, *gsc*), the posterior larval tip and chaetae (*fer3*, *lhx1/5*, *wnt1*, *notch*, *msx2-a*, *irxA*, *AP2*, *wnt4*, *delta*), the hindgut (*cdx*), or mesodermal derivatives (*foxH*, *rhox*, *wntA*, *POU3*, *hand2*, *twist*) (Figure 3D,

Figure S4). Analysis of the expression of these genes in control and treated embryos at the coeloblastula (5.5hpf) and larva (24hpf) stages confirmed the expression domains of these genes disappear after treatment with either BFA or U0126 (Figure 3E, Figure S4), thus validating our RNA-seq approach. Altogether, these results define a set of co-regulated genes that act downstream of ERK1/2 signalling and/or early inductive events, and that are involved in the development of apical, posterodorsal and mesodermal structures in *O. fusiformis*.

ERK1/2 signalling specifies and patterns the D-quadrant

Our RNA-seq study and candidate gene screening revealed nine genes expressed at the vegetal pole at 5.5 hpf and whose expression was affected by either direct inhibition of ERK1/2 di-phosphorylation (*cdx*, *delta*, *foxH*, *wnt1*, *wntA*, *rhox*, *fer3* and *AP2*) or impairing cell-to-cell inductive signals (*gsc*) (Figure 3E, Figure S4). None of these genes are expressed at 5 hpf, at the onset of ERK1/2 activity in the 4d micromere (Figure 4A). Instead, the early endodermal marker *GATA4/5/6a* [39], whose expression is unaffected by BFA and U0126 treatment and thus is cell-autonomous, is symmetrically expressed in the gastral plate (including 4d) at this stage (Figure 4A; Figure S5A). At 5.5 hpf, half an hour after the initial activation of ERK1/2 signalling in 4d, the vegetal pole becomes bilaterally symmetrically patterned, but only two of the ERK1/2 dependent genes (*cdx* and *delta*) are expressed in the 4d micromere (Figure 4A). The ParaHox gene *cdx*, which is detected in the hindgut of *O. fusiformis* at the larval stage [39] (Figure 3E; Figure S5B), becomes expressed in 4d, and later on in two cells of the MR and ML progeny at the gastrula stage (Figure 4B), as expected from the behaviour of 4d at these stages (Figure 1E). Similarly, the Notch ligand *delta* (Figure S5C, D) is expressed in 4d at 5.5 hpf, but also in most of the descendants of 1d at the animal pole, plus 1a–c[1121] and ectodermal derivatives of the C and D quadrant at the vegetal pole (Figure 4A, C). To investigate how ERK1/2 might control activation of *cdx* and *delta*, we used Assay

for Transposase-Accessible Chromatin using sequencing (ATAC-seq) data at 5 hpf and identified known bound transcription factors in the accessible regions associated with these genes (Figure 4D), which include DNA binding motifs for transcription factors known to be modulated by ERK1/2 phosphorylation, such as ETS, RUNX and GATA factors [15]. Therefore, ERK1/2 di-phosphorylation in 4d seems to delay cell cycle progression in this cell with respect to 4a–c (Figure 1E) and control the activity of transcriptional regulators that induce posterior fates (*cdx*) and cell-cell communication genes (*delta*).

The other six additional ERK1/2-dependent genes pattern the micromeres surrounding 4d at 5.5 hpf, defining mesodermal and posterior ectodermal domains (Figure 4A). The transcription factor *foxH* (Figure S5E), which regulates mesoderm development during gastrulation in vertebrate embryos [40-43], is detected in the $3c^{22}$ and $3d^{22}$ micromeres adjacent to 4d (Figure 4A), whose progeny contributes to lateral ectomesoderm in the annelid *Urechis caupo* [36]. Later in development, *foxH* is expressed in a posterior V-shaped pattern of putative mesodermal precursors during axial elongation, fading away in larval stages (Figure S5B). The ligands *wnt1* and *wntA* (Figure S5), expressed in the posterior region and D-quadrant during development in the annelid *Platynereis dumerilii* [44], are expressed in two bilaterally symmetrical columns of micromeres ($3c^{22}$, $3c^{21}$, $3c^{12}$, $3c^{11}$, $3d^{22}$, $3d^{21}$, $3d^{12}$, $3d^{11}$) plus the micromeres $2d^{222}$ and $2d^{112}$ in *wntA* (Figure 4A). The homeobox *rhox* (Figure S5G), which is expressed in male and female primordial germ cells in vertebrates [45], is detected in the micromeres $2d^{112}$ and $2d^{212}$ (Figure 4A) and thereafter in two small cells inside the blastocele in the gastrula (Figure S4). The transcription factors *fer3* and *AP2* are expressed in two single micromeres ($1c^{222}$ and $1d^{221}$) and in a broader posterior ectodermal domain ($1c^{222}$, $1d^{221}$, $2d^{122}$, $2d^{212}$, $2d^{2111}$, $2d^{2112}$, $2d^{1112}$, $2d^{1111}$) respectively, becoming restricted to a small expression domain at or near the posterior chaetal sac of the larva (Figure S4; Figure

S5B). The larger size of 4d, which stays as a big posterior cell at 5.5 hpf, allows it to establish almost as double direct cell-cell contacts with its surrounding cells than each of the daughter cells of 4a–c, including most of the cells expressing *foxH*, *wnt1*, *wntA*, *rhox*, and *AP2* (Figure 4E). This data demonstrates the inductive role of the 4d in defining mesodermal and posterodorsal fates, and together with the upregulation of the Notch-ligand *delta* in 4d after ERK1/2 activation, suggests that this role might occur by direct cell-cell communication mediated by the Notch signalling pathway.

The homeobox gene *gsc* is the only candidate expressed outside the D-quadrant at 5.5 hpf, being detected in micromeres $2a^{11}$–$2c^{11}$, $2a^{12}$–$2c^{12}$, $2a^{21}$–$2c^{21}$, and $2a^{22}$–$2c^{22}$ (Figure 4A). Consistent with its location outside the D-quadrant, *gsc* expression is independent of ERK1/2 activity, but requires of inductive signals, as demonstrated by being downregulated after BFA treatment (Table S3). Accordingly, *gsc* expression disappears in BFA-treated coeloblastulae, while inhibition of ERK1/2 activity with U0126 expands *gsc* domains, which becomes detected in all embryonic quadrants in a radial fashion (Figure 4F). Indeed, in ERK1/2 inhibited embryos all 4q micromeres cleave into $4q^1$ and $4q^2$, as no 4q becomes the 4d cell (Figure 4F). Therefore, all quadrants adopt antero-ventral fates (*gsc*), preventing the expression of posterior marker genes such as *AP2* (Figure 4F). These results demonstrate that the radial phenotype observed after U0126 is a consequence of misspecifying the 4d cell, and not a result of the D-quadrant becoming specified but not developing further. In addition, this data also demonstrates that specification of the 4d cell through ERK1/2 activity represses anterior fates, as shown by limiting *gsc* expression.

FGF signalling regulates ERK1/2 di-phosphorylation in 4d

In *O. fusiformis*, *cdx* and *delta* are expressed in 4d under regulation of ERK1/2, and their expression is associated with hindgut and trunk mesoderm development, as well as posterior growth (Figure 2C). In vertebrate embryos, FGF signalling mediated by ERK1/2 activity regulates the expression of *cdx* and *delta* in the developing hindgut and presomitic mesoderm during posterior elongation [46] and FGF signalling promotes mesoderm development in the spiralian groups Brachiopoda and Phoronida [47]. We thus hypothesised that FGF signalling might be the upstream regulator driving ERK1/2 activity in 4d (Figure 5A). *O. fusiformis* has a single FGF receptor (FGFR; Figure S6A) with high amino acid conservation at key functional residues compared to the human FGFR1 ortholog (Figure 6B). While it is transcriptionally upregulated at the gastrula stage, *FGFR* appears weakly expressed at the gastral plate at the coeloblastula stage in *O. fusiformis* (Figure S6C, D), as observed in brachiopods and phoronids [47]. At this stage, FGF ligands and VEGFR, the other tyrosine kinase receptor inhibited by SU5402, are only weakly expressed (Figure S6C) and not detected by *in situ* hybridisation (Figure S6D). Treatment with 30 µM SU5402, a selective inhibitor of FGFR phosphorylation and activation [48] (Figure 5A), prevents di-P-ERK1/2 enrichment at 4d cell in 96% of the treated embryos at 5 hpf (Figure 5B, Figure S6E, Table S2). Indeed, treatment with SU5402 during the specification of the 4d micromere (4 to 6 hpf and 3 to 7 hpf; Figure 5C) results in an anteriorly radialised phenotype, with embryos developing into larvae lacking posterior and reduced mesodermal structures and showing radially expended oral ectodermal fates (*gsc*) (Figure 5D, Table S3). Conversely, treatment before di-P-ERK1/2 enrichment in 4d (3 to 5 hpf) causes a slightly compressed phenotype (Figure S6F). Therefore, inhibition of FGFR blocks ERK1/2 activation and phenocopies the effect of U0126 and BFA (Figure 2C), suggesting that FGF signalling activity is upstream of and necessary for 4d specification in *O. fusiformis*.

Discussion

Our study provides compelling evidence that FGFR and ERK1/2 signalling specify and control the organising activity of the 4d micromere in the conditional spiral cleaving annelid *O. fusiformis* (Figure 6A). FGFR/ERK1/2 signalling at around 5 hpf is necessary for instructing one of the recently emerged 4q micromeres into the D fate (Figure 2E, Figure 5C, Figure 6A). However, 4q micromeres form already asymmetrically at 4 hpf in *O. fusiformis* (Figure 1E), yet whether there is an exact correspondence between the order of formation and the fate of each 4q remains elusive. Asynchronies in the cleavage of 3Q have not been described for other conditional cleaving annelids [33-35], but are more common in molluscs, where 4d can be either the first or the last micromere to form [3, 12, 14]. This asynchrony in 3Q cleavage, together with the fact that ERK1/2 signalling affects axial polarity independently of cell communication (i.e., unaffected by BFA) earlier than 4 hpf (Figure 2E, Figure S2C) suggest that cell-autonomous ERK1/2-dependent mechanisms might act before the inductive specification of 4d in *O. fusiformis*. In other systems, MAPK controls unequal protein segregation during mitosis via pericentrosomal material [49], which is the subcellular region where maternal mRNAs condense before asymmetric inheritance during spiral cleavage in the mollusc *Tritia obsoleta* [50], and MAPK controls mRNA stability during early zygotic divisions in the annelid *Helobdella robusta* [51]. Therefore, basal levels of ERK1/2 signalling during early cleavage might control the activity or differential segregation of determinants required to respond adequately to the inductive signals specifying the 4d cell in *O. fusiformis*. Although further work is needed to test this scenario, our findings indicate that both autonomous and conditional mechanisms are essential to specify the D-quadrant organiser in *O. fusiformis*, challenging traditional views that conditional/equal spiral cleaving species rely mostly on inductive signals to establish their body pattern.

The specification of 4d micromere has at least four immediate consequences during *O. fusiformis* embryogenesis (Figure 6A). First, and contrary to its role in promoting cell proliferation [15], ERK1/2 activity correlates with 4d cell cycle arrest, breaking the quatri-radial symmetry of the embryo as the 4a–4c micromeres cleave (Figure 1E; Figure 6A). In some molluscs, activation of ERK1/2 in the 3D blastomere also correlates with cleavage delays [12, 17], and thus a potential role of ERK1/2 signalling in arresting, instead of promoting, cell division appears to be common in the context of the embryonic organiser in spiralian embryos. Second, specification of 4d and the D-quadrant represses anterior fates to the A–C quadrants, as observed by the expression of the BFA-affected oral ectodermal gene *gsc* in all four quadrants in ERK1/2 inhibited embryos (Figure 4F). These findings suggest that two as yet unknown opposing signals – one specifying anterior fates and promoting *gsc* expression, and another driving 4d specification via FGFR/ERK1/2 – might act simultaneously at 4–5 hpf (Figure 6A). Considering that *gsc* expression is eventually recovered in BFA treated larvae (Figure S2C), we hypothesise that this anteriorising signal must come from cell lineages already specified by 4–5 hpf, such as the endoderm/midgut (Figure 4A) or the apical organ (Figure 2D). Third, FGF/ERK1/2 activity upregulates the hindgut gene *cdx* in 4d (Figure 3C; Figure 4A; Figure 6A). Inhibition of both FGF and ERK1/2 activity affects hindgut but not foregut and midgut development (Figure 2C; Figure 5D), indicating that unlike most annelids [21] but similar to molluscs [3, 52], 4d contributes to both endoderm/hindgut and mesoderm in *O. fusiformis*. Fourth, FGF/ERK1/2 activity also upregulates the Notch ligand *delta* in 4d, as well as a set of mesodermal and posterior genes, Wnt ligands and TGF-β modulators in its surrounding cells, most of which establish a direct cell-to-cell contact with 4d (Figure 4A, E; Figure 6A). Therefore, 4d instructs cell fates in the D and C quadrant at the vegetal pole, probably through the Notch signalling pathway, as also

proposed for the mollusc *Tritia obsoleta* [53]. Altogether, our study demonstrates the organising properties of the 4d cell (endomesodermal precursor) in *O. fusiformis*, defining a comprehensive, testable model to study the establishment of the body plan in this and other spiral cleaving organisms.

Enrichment of di-phosphorylated ERK1/2 in the 4d micromere is common to *O. fusiformis* and *H. hexagonus*, the two conditional spiral cleaving annelids studied so far [17], which contrasts with the variability in ERK1/2 activity observed among autonomous cleaving annelids [25-27]. Likewise, the 4d cellular identity of the D-quadrant organiser in *O. fusiformis* differs from the autonomous annelid species *C. teleta* and *T. tubifex*, which concentrate the organising activity in the 2d and $2d^{11}$ + 4d cells respectively [26, 28]. However, the 4d cell identity observed in *O. fusiformis* resembles the molluscan condition, where ERK1/2 is active in 3D and maintained in 4d, both of which can exert organising activity [9, 12]. Moreover, *cdx* and *delta*, the downstream targets of ERK1/2 in the 4d of *O. fusiformis*, are also expressed in 4d in the mollusc *Tritia obsoleta* [52, 53], further suggesting conservation in both signalling cascades and transcriptional outputs between D-quadrant organisers in annelids and molluscs. Therefore, our study supports that ERK1/2 activity in the cell acting as embryonic organiser is a shared homologous trait between Annelida and Mollusca and given our current understanding of Spiralia phylogeny [6, 7], a probable ancestral character to at least the internal node Lophotrochozoa. Under this scenario, heterochronic shifts to confer organising activity to 2d micromeres as seen in *C. teleta* and *T. tubifex* [26, 28] and the use of Activin/Nodal signalling instead of ERK1/2 to establish the body plan [24, 29] are thus derived conditions.

More broadly, our study uncovers a role of the FGF signalling pathway, an evolutionarily conserved upstream regulator of mesoderm development in bilaterians [47, 54, 55], in the specification of 4d, the D-quadrant organiser and endomesodermal precursor in *O. fusiformis* (Figure 5B–D). FGFR activity in 4d results in the activation of *cdx*, Notch signalling (*delta*) and Wnt signalling (*wnt1*, *wntA*) in vegetal micromeres of the D-quadrant (Figure 4A) that will occupy the posterodorsal blastoporal lip as gastrulation begins, supporting that blastopore-associated axial organisers also occur during spiral cleavage [4]. Furthermore, FGF, Wnt and Notch signalling, together with *cdx* are all conserved gene modules regulating posterior axis elongation in an array of bilaterian embryos (Figure 6B) [39, 46, 47, 56-58]. Classically, axial elongation in spiralian embryos has been proposed to occur by proliferation of the 2d clone [59, 60], which express *delta* and *wntA* in *O. fusiformis* (Figure 4A), further suggesting that specification of 4d also results in the deployment of broadly conserved genetic mechanisms involved in posterior growth that eventually promote axial (and blastopore) elongation in *O. fusiformis* (Figure 2C; Figure 6B). Altogether, our study demonstrates that the establishment of the axial identities (A–D quadrants), endomesoderm specification, posterodorsal patterning and axial elongation are all intimately connected events that depend on the instruction of a single cell fate (the 4d cell) and use evolutionarily conserved mechanisms in *O. fusiformis*, a conditional spiral cleaving annelid. Decoupling these embryonic organising processes through maternal determinants (e.g., as in autonomous spiral cleavers), heterochronic shifts in organiser specification and/or signalling pathway rewiring (e.g., co-option of Activin/Nodal) might have thus contributed to the emergence of the vast diversity of body plans observed today in Spiralia.

Acknowledgements

We thank the staff at Station Biologique de Roscoff for their help with collections and animal supplies, as well as the Oxford Genomics Centre at the Wellcome Centre for Human Genetics (funded by Wellcome Trust grant reference 203141/Z/16/Z) for the generation and initial processing of RNA-seq and ATAC-seq sequencing data. We thank all members of the Martín-Durán lab for support and valuable comments on the manuscript. This work was funded by a European Research Council Starting Grant (action number 801669) to J.M.M.-D. and a Queen Mary, University of London studentship to O.S.

Author Contributions

O.S., A.M.C.-B. and J.M.M.-D. conceived and designed the study. O.S., A.M.C.-B., Y.L. and J.M.M.-D. performed all experimental approaches and critically analysed the data. O.S., A.M.C.-B. and J.M.M.-D. wrote the manuscript. All authors read and commented on the manuscript.

Declaration of Interests

The authors declare no competing interests.

Materials and Methods

Animal husbandry and embryo collections

Adult specimens of *O. fusiformis* Delle Chiaje, 1844 were collected from the coast near the Station Biologique de Roscoff (France) during the reproductive season (May to July). In the lab, animals were kept in artificial seawater (ASW) at 15°C. *In vitro* fertilizations were conducted as previously described [31, 39] and embryos develop in glass bowls with filtered ASW at 19 ºC until the desired embryonic stage.

Drug treatments

Embryos were treated with either brefeldin A (BFA; Sigma-Aldrich, #B7651), U0126 (Sigma-Aldrich, #U120), or SU5402 (Sigma-Aldrich, #572630). All drug stocks were made in dimethyl sulfoxide (DMSO) and diluted in ASW prior use, with optimal working concentrations (10 µM for BFA and U0126 and 30 µM for SU5402) established after initial titration. For all drug treatments, equivalent volumes of DMSO were used as negative control, and in all cases, treatments were initiated after ~0.5 hours post fertilisation (hpf), right after fertilisation and sperm removal. Treatments were stopped by washing out the drug with at least three washes in ASW and embryos were either collected for downstream analyses or raised until larval stage. Samples collected for immunohistochemistry and gene expression analyses were fixed in 4% paraformaldehyde (PFA) in ASW for 1h at room temperature (RT). Larvae were relaxed in 8% magnesium chloride ($MgCl_2$) prior fixation and fixed in 4% PFA in 8% $MgCl_2$ for 1h at RT. After fixation, samples were washed several times with 0.1% Tween-20 phosphate-buffered saline (PTw), and either stored in PTw at 4°C for immunohistochemistry or dehydrated to 100% methanol and stored at -20°C for whole mount *in situ* hybridisation. Treated and control embryos and larvae collected for RNA-seq analyses were snap frozen in liquid nitrogen and stored at -80°C prior total RNA extraction.

Immunohistochemistry

F-actin labelling, and antibody staining were conducted as previously described [31], with the modification that samples collected for anti-di-P-ERK1/2 staining were washed in PTw supplemented with 1:100 dilution of phosphatase inhibitors (Cell Signalling, #5872) after fixation. The primary antibodies mouse anti-double phosphorylated ERK1/2 (Sigma-Aldrich, #M8159, 1:200) and mouse anti-acetylated α-tubulin (clone 6-11B-1, Millipore-446 Sigma, #MABT868, 1:500) were diluted in 5% normal goat serum (NGS) in 0.1% Triton X-100 phosphate-buffered saline (PTx) and incubated overnight (ON) at 4 °C. After several washes in 1% bovine serum albumin (BSA) in PTx, samples were incubated with either an anti-mouse peroxidase (POD) conjugated antibody (Millipore-Sigma, #11207733910, 1:100) or an AlexaFluor594 conjugated antibody (ThermoFisher Scientific, #A32731) diluted in 5% NGS in PTx ON at 4ºC. For samples incubated with mouse anti-double phosphorylated ERK1/2 and anti-mouse POD conjugated antibody, signal was developed using either diaminobenzidine (DAB) (Vector Laboratories, #SK-4100) or Tyramide Signal Amplification (TSA) kit (Akoya Biosciences, #NEL742001KT) following manufacturer's recommendations. DAB-developed samples were stored in 70% glycerol and counterstained with 4',6-diamidino-2- phenylindole (DAPI, ThermoFisher Scientific, #D3571, 1:1000) nuclear marker. Samples for laser scanning confocal microscopy (LSCM) were counterstained with DAPI diluted in 1% bovine serum albumin (BSA) in PTx for 1h at RT and mounted in 70% glycerol.

Gene isolation and gene expression analyses

Candidate genes were amplified by two rounds of nested PCR using gene specific primers and a T7 universal primer on cDNA from mixed developmental stages as initial template (Table

S9). Riboprobes were synthesized with the T7 enzyme (Ambion's MEGAscript kit, #AM1334) and stored in hybridisation buffer at a concentration of 50 ng/µl. Colorimetric and fluorescent whole-mount *in situ* hybridisation were performed following an established protocol [31, 39]. After probe washes, samples for fluorescent *in situ* hybridisation were incubated with anti-DIG-POD Fab fragments (ROCHE, #11633716001) and a mouse anti-acetylated α-tubulin antibody (clone 6-11B-1, Millipore-446 Sigma, #MABT868, 1:500) to co-stain cell boundaries. After signal development with the TSA kit (Akoya Biosciences, #NEL742001KT), these samples were washed several times in PTx and treated for secondary antibody incubation as described above.

Genome sequencing, gene annotation and RNA-seq developmental time course

High molecular weight genomic DNA was obtained from a single *O. fusiformis* male following the agar plug extraction method and sequenced on a PacBio Sequel II platform to a ~200x coverage. Initial assembly was conducted with Canu [61], subsequently scaffolded with BioNano optical mapping data generated on an Irys platform and finally de-haploidised with purge_haplotigs [62]. To annotate protein coding genes, we used available transcriptomic data (SRA accession number SRR1222288) and generated replicated stage-specific RNA-seq data covering twelve developmental time-points, from the unfertilized active oocyte until the mature mitraria larva. RNA-seq reads were mapped with STAR [63] and gene models were generated combining Mikado v.2.1 [64], Augustus [65] and PASA [66] pipelines. Gene completeness was assessed with BUSCO [67] (97.5% complete, 1.5% fragmented, 1% missing). Trinotate [68] and Panther [69] were used to functionally annotate gene predictions and obtain initial gene orthology assignments. To identify gene expression dynamics during development, we used the stage specific RNA-seq generated for annotation, representing the average expression of the two replicates with the package pheatmap v.1.0.12

available in R, were colour intensity shows the z-score value for each gene. All raw sequencing data is available under the project with accession number XXXXXX in the European Nucleotide Archive (ENA).

Assay for Transposase-Accessible Chromatin using sequencing (ATAC-seq)

Two replicated ATAC-seq libraries were generated from >50,000 cells at 5 hpf (850-900 coeloblastulae) following the Omni-ATAC protocol [70], employing a home-made Tn5 transposase [71] and amplifying for 12 cycles. Libraries were sequenced on an Illumina Hiseq4000 platform, 75 base paired-end output mode. After adaptor removal with cutadapt v.2.5 [72], reads were mapped with NextGenMap v.0.5.5 [73] and duplicates removed with samtools v.1.9 [74]. BAM files were shifted using deepTools2 v.3.4.3 [75] and MACS2 v2.2.7.1 [76, 77] was used for peak calling with parameters -f BAMPE --min-length 100 --max-gap 75 -q 0.01. Reproducible peaks ($p < 0.05$) were identified applying Irreproducible Discovery Rate package v2.0.4.2 [78]. Transcription factor motif enrichment was performed with HOMER v.4.11 [79] and transcription factor foot printing with TOBIAS v.0.12.0 [80]. To identify bound transcription factors on peaks of *cdx* and *delta*, we intersected the genomic positions of peaks and bound transcription factors with BEDTools v.2.29.2 [81]. Genomic tracks were plotted with pyGenomeTracks v.2.1 [82].

RNA-seq profiling and differential gene expression analyses

Total RNA was extracted using the Monarch total RNA Miniprep Kit (New England Biolabs, #T2010) and used for Illumina stranded mRNA library prep. Sequencing was performed on an Illumina HiSeq 4000 platform in 75 bases paired-end output mode, generating ~20 million reads per sample. Adapter sequences and low-quality bases were removed using Trimmomatic v.0.36 [83]. Cleaned reads were then mapped to *O.*

fusiformis reference genome annotation using Kallisto v.0.44.0 to generate gene expression counts [84]. Differential gene expression analyses were performed independently for each drug and computed in pairwise comparisons of different stages and conditions using the R package DEseq2 v.1.38.0 [85]. Significancy threshold was adjusted to a p-value equal or lower than 0.05 and a Log2 fold change greater than 1.5 or lower than -1.5 [86]. PCAs and hierarchical clustering were plotted using ggplot2 and pheatmap R packages, respectively [87]. Volcano plots were obtained with the package EnhancedVolcano, available in R. Candidate genes for further gene expression analyses were selected based on being differentially expressed in both drug treatments (U0126 and BFA) or highly differentially expressed at 5.5 hpf in U0126 treated embryos. We further refined our selection based on gene ontology (GO) categories, focusing on transcription factors and developmental genes (Table S7).

GO and KEGG enrichment analyses

For GO mapping, the GO terms of differentially expressed genes (DEGs) associated with each comparison were extracted from *O. fusiformis* reference genome annotation. GO enrichment analyses were implemented using the GOseq R package, correcting for gene length bias [88], and analysing up-regulated and down-regulated genes independently. GO terms with corrected p-values lower than 0.05 were considered to be significantly enriched (Table S7). A similar approach was followed for Kyoto Encyclopaedia of Genes and Genomes (KEGG) pathway enrichment analyses, mapping differentially represented KO numbers to their respective KEGG pathway [89] (Table S8).

Orthology assignment and domain architecture analyses

Generally, gene orthology was based on the functional annotation of *O. fusiformis* gene repertoire, based on BLAST searches against SwissProt database and Panther searches [69, 90]. Protein sequences for ERK1/2 and ERK5, WNT ligands, RHOX and related homeoboxes, DLL and JAGGED, FOXH and FOXF genes and FGFR and VEGFR were retrieved by mining publicly available transcriptomes and databases. Multiple protein alignments (Supplementary File 1) were constructed with MAFFT v.7 in automatic mode [91] and poorly aligned regions were removed with gBlocks version 0.91b [92]. Maximum likelihood trees were constructed with either RAxML v.8.2.11 [93] or FastTree [94] and visualised with FigTree (https://github.com/rambaut/figtree/). InterProScan 5 [95] was used to perform the protein domain composition of DLL.

Imaging

Representative embryos and larvae from colorimetric analyses were imaged with a Leica DMRA2 upright epifluorescent microscope equipped with an Infinity5 camera (Lumenera), using bright field and differential interference contrast optics. Fluorescently stained samples were scanned with a Leica SP5 LSCM. Confocal stacks were analysed with Fiji and brightness/contrast and colour balance were adjusted in Pixelmator Pro (v. 2.0.3) or Photoshop (Adobe), applying changes always to the whole image and not parts of it. Final figures were designed using Illustrator (Adobe).

References

1. Martinez Arias, A., and Steventon, B. (2018). On the nature and function of organizers. Development *145*.
2. Anderson, C., Khan, M.A.F., Wong, F., Solovieva, T., Oliveira, N.M.M., Baldock, R.A., Tickle, C., Burt, D.W., and Stern, C.D. (2016). A strategy to discover new organizers identifies a putative heart organizer. Nat Commun *7*, 12656.
3. Lyons, D.C., Perry, K.J., Lesoway, M.P., and Henry, J.Q. (2012). Cleavage pattern and fate map of the mesentoblast, 4d, in the gastropod *Crepidula*: a hallmark of spiralian development. Evodevo *3*, 21.
4. Kraus, Y., Aman, A., Technau, U., and Genikhovich, G. (2016). Pre-bilaterian origin of the blastoporal axial organizer. Nat Commun *7*, 11694.
5. Lapraz, F., Haillot, E., and Lepage, T. (2015). A deuterostome origin of the Spemann organiser suggested by Nodal and ADMPs functions in Echinoderms. Nat Commun *6*, 8434.
6. Laumer, C.E., Bekkouche, N., Kerbl, A., Goetz, F., Neves, R.C., Sorensen, M.V., Kristensen, R.M., Hejnol, A., Dunn, C.W., Giribet, G., et al. (2015). Spiralian phylogeny informs the evolution of microscopic lineages. Curr Biol *25*, 2000-2006.
7. Marlétaz, F., Peijnenburg, K., Goto, T., Satoh, N., and Rokhsar, D.S. (2019). A New Spiralian Phylogeny Places the Enigmatic Arrow Worms among Gnathiferans. Curr Biol *29*, 312-318 e313.
8. Martín-Durán, J.M., and Marletaz, F. (2020). Unravelling spiral cleavage. Development *147*.
9. Henry, J.Q. (2014). Spiralian model systems. Int J Dev Biol *58*, 389-401.
10. Hejnol, A. (2010). A twist in time--the evolution of spiral cleavage in the light of animal phylogeny. Integr Comp Biol *50*, 695-706.

11. Schleip, W. (1929). Die Determination der Primitiventwicklung, (Leipzig: Akademische Verlagsgesellschaft).

12. Lambert, J.D. (2008). Mesoderm in spiralians: the organizer and the 4d cell. J Exp Zool B Mol Dev Evol *310*, 15-23.

13. Freeman, G., and Lundelius, J.W. (1992). Evolutionary implications of the mode of D quadrant specification in coelomates with spiral cleavage. Journal of Evolutionary Biology *5*, 205-247.

14. Van Den Biggelaar, J.A.M., Van Loon, A.E., and Damen, W.G.M. (1995). Mesentoblast and Trochoblast Specification in Species With Spiral Cleavage Predict Their Phyletic Relations. Netherlands Journal of Zoology *46*, 8-21.

15. Lavoie, H., Gagnon, J., and Therrien, M. (2020). ERK signalling: a master regulator of cell behaviour, life and fate. Nat Rev Mol Cell Biol *21*, 607-632.

16. Lambert, J.D., and Nagy, L.M. (2001). MAPK signaling by the D quadrant embryonic organizer of the mollusc *Ilyanassa obsoleta*. Development *128*, 45-56.

17. Lambert, J.D., and Nagy, L.M. (2003). The MAPK cascade in equally cleaving spiralian embryos. Dev Biol *263*, 231-241.

18. Lartillot, N., Lespinet, O., Vervoort, M., and Adoutte, A. (2002). Expression pattern of *Brachyury* in the mollusc *Patella vulgata* suggests a conserved role in the establishment of the AP axis in Bilateria. Development *129*, 1411-1421.

19. Henry, J.J., and Perry, K.J. (2008). MAPK activation and the specification of the D quadrant in the gastropod mollusc, *Crepidula fornicata*. Dev Biol *313*, 181-195.

20. Koop, D., Richards, G.S., Wanninger, A., Gunter, H.M., and Degnan, B.M. (2007). The role of MAPK signaling in patterning and establishing axial symmetry in the gastropod *Haliotis asinina*. Dev Biol *311*, 200-212.

21. Ozpolat, B.D., Handberg-Thorsager, M., Vervoort, M., and Balavoine, G. (2017). Cell lineage and cell cycling analyses of the 4d micromere using live imaging in the marine annelid *Platynereis dumerilii*. Elife *6*.

22. Gline, S.E., Nakamoto, A., Cho, S.J., Chi, C., and Weisblat, D.A. (2011). Lineage analysis of micromere 4d, a super-phylotypic cell for Lophotrochozoa, in the leech *Helobdella* and the sludgeworm *Tubifex*. Dev Biol *353*, 120-133.

23. Meyer, N.P., Boyle, M.J., Martindale, M.Q., and Seaver, E.C. (2010). A comprehensive fate map by intracellular injection of identified blastomeres in the marine polychaete *Capitella teleta*. Evodevo *1*, 8.

24. Lanza, A.R., and Seaver, E.C. (2020). Activin/Nodal signaling mediates dorsal-ventral axis formation before third quartet formation in embryos of the annelid *Chaetopterus pergamentaceus*. Evodevo *11*, 17.

25. Pfeifer, K., Schaub, C., Domsch, K., Dorresteijn, A., and Wolfstetter, G. (2014). Maternal inheritance of *twist* and analysis of MAPK activation in embryos of the polychaete annelid *Platynereis dumerilii*. PLoS One *9*, e96702.

26. Amiel, A.R., Henry, J.Q., and Seaver, E.C. (2013). An organizing activity is required for head patterning and cell fate specification in the polychaete annelid *Capitella teleta*: new insights into cell-cell signaling in Lophotrochozoa. Dev Biol *379*, 107-122.

27. Kozin, V.V., Filimonova, D.A., Kupriashova, E.E., and Kostyuchenko, R.P. (2016). Mesoderm patterning and morphogenesis in the polychaete *Alitta virens* (Spiralia, Annelida): Expression of mesodermal markers *Twist*, *Mox*, *Evx* and functional role for MAP kinase signaling. Mech Dev *140*, 1-11.

28. Nakamoto, A., Nagy, L.M., and Shimizu, T. (2011). Secondary embryonic axis formation by transplantation of D quadrant micromeres in an oligochaete annelid. Development *138*, 283-290.

29. Lanza, A.R., and Seaver, E.C. (2020). Functional evidence that Activin/Nodal signaling is required for establishing the dorsal-ventral axis in the annelid *Capitella teleta*. Development *147*.

30. Weigert, A., Helm, C., Meyer, M., Nickel, B., Arendt, D., Hausdorf, B., Santos, S.R., Halanych, K.M., Purschke, G., Bleidorn, C., et al. (2014). Illuminating the base of the annelid tree using transcriptomics. Mol Biol Evol *31*, 1391-1401.

31. Carrillo-Baltodano, A.M., Seudre, O., Guynes, K., and Martin-Duran, J.M. (2021). Early embryogenesis and organogenesis in the annelid *Owenia fusiformis*. Evodevo *12*, 5.

32. Gonzales, E.E., van der Zee, M., Dictus, W.J., and van den Biggelaar, J. (2007). Brefeldin A and monensin inhibit the D quadrant organizer in the polychaete annelids *Arctonoe vittata* and *Serpula columbiana*. Evol Dev *9*, 416-431.

33. Treadwell, A.L. (1901). The cytogeny of *Podarke obscura* Verrill. J. Morph. *17*, 399-478.

34. Mead, A.D. (1897). The early development of marine annelids. J. Morph. *13*, 227-326.

35. Woltereck, R. (1904). Beiträge zur praktischen Analyse der *Polygordius*-Entwicklung nach dem 'Nordsee' - und dem 'Mittelmeer-typus'. I. Der für beide Typen gleich verlaufende Entwicklungsabschnitt: vom Ei bis zum jüngsten Trochophora-Stadium. Arch. f. Entwicklungsmech. *18*, 377-403.

36. Newby, W.W. (1940). The embryology of the echiuroid worm *Urechis caupo*, Volume 16, (Philadelphia: The American Philosophical Society).

37. Gonzales, E.E., van der Zee, M., Dictus, W.J., and van den Biggelaar, J. (2007). Brefeldin A or monensin inhibits the 3D organizer in gastropod, polyplacophoran, and scaphopod molluscs. Dev Genes Evol *217*, 105-118.

38. Favata, M.F., Horiuchi, K.Y., Manos, E.J., Daulerio, A.J., Stradley, D.A., Feeser, W.S., Van Dyk, D.E., Pitts, W.J., Earl, R.A., Hobbs, F., et al. (1998). Identification of a novel inhibitor of mitogen-activated protein kinase kinase. J Biol Chem *273*, 18623-18632.

39. Martin-Duran, J.M., Passamaneck, Y.J., Martindale, M.Q., and Hejnol, A. (2016). The developmental basis for the recurrent evolution of deuterostomy and protostomy. Nat Ecol Evol *1*, 5.

40. Hoodless, P.A., Pye, M., Chazaud, C., Labbe, E., Attisano, L., Rossant, J., and Wrana, J.L. (2001). FoxH1 (Fast) functions to specify the anterior primitive streak in the mouse. Genes Dev *15*, 1257-1271.

41. Pogoda, H.M., Solnica-Krezel, L., Driever, W., and Meyer, D. (2000). The zebrafish forkhead transcription factor FoxH1/Fast1 is a modulator of nodal signaling required for organizer formation. Curr Biol *10*, 1041-1049.

42. Yamamoto, M., Meno, C., Sakai, Y., Shiratori, H., Mochida, K., Ikawa, Y., Saijoh, Y., and Hamada, H. (2001). The transcription factor FoxH1 (FAST) mediates Nodal signaling during anterior-posterior patterning and node formation in the mouse. Genes Dev *15*, 1242-1256.

43. Watanabe, M., and Whitman, M. (1999). FAST-1 is a key maternal effector of mesoderm inducers in the early Xenopus embryo. Development *126*, 5621-5634.

44. Pruitt, M.M., Letcher, E.J., Chou, H.C., Bastin, B.R., and Schneider, S.Q. (2014). Expression of the wnt gene complement in a spiral-cleaving embryo and trochophore larva. Int J Dev Biol *58*, 563-573.

45. MacLean, J.A., 2nd, and Wilkinson, M.F. (2010). The Rhox genes. Reproduction *140*, 195-213.

46. Hubaud, A., and Pourquié, O. (2014). Signalling dynamics in vertebrate segmentation. Nat Rev Mol Cell Biol *15*, 709-721.

47. Andrikou, C., and Hejnol, A. (2021). FGF signaling acts on different levels of mesoderm development within Spiralia. Development.

48. Sun, L., Tran, N., Liang, C., Tang, F., Rice, A., Schreck, R., Waltz, K., Shawver, L.K., McMahon, G., and Tang, C. (1999). Design, Synthesis, and Evaluations of Substituted 3-[(3- or 4-Carboxyethylpyrrol-2-yl)methylidenyl]indolin-2-ones as Inhibitors of VEGF, FGF, and PDGF Receptor Tyrosine Kinases. Journal of Medicinal Chemistry *42*, 5120-5130.

49. Fuentealba, L.C., Eivers, E., Geissert, D., Taelman, V., and De Robertis, E.M. (2008). Asymmetric mitosis: Unequal segregation of proteins destined for degradation. Proc Natl Acad Sci U S A *105*, 7732-7737.

50. Lambert, J.D., and Nagy, L.M. (2002). Asymmetric inheritance of centrosomally localized mRNAs during embryonic cleavages. Nature *420*, 682-686.

51. Gonsalves, F.C., and Weisblat, D.A. (2007). MAPK regulation of maternal and zygotic Notch transcript stability in early development. Proc Natl Acad Sci U S A *104*, 531-536.

52. Johnson, A.B., and Lambert, J.D. (2021). The Caudal ParaHox gene is required for hindgut development in the mollusc *Tritia* (a.k.a. *Ilyanassa*). Dev Biol *470*, 1-9.

53. Gharbiah, M., Nakamoto, A., Johnson, A.B., Lambert, J.D., and Nagy, L.M. (2014). *Ilyanassa* Notch signaling implicated in dynamic signaling between all three germ layers. Int J Dev Biol *58*, 551-562.

54. Dorey, K., and Amaya, E. (2010). FGF signalling: diverse roles during early vertebrate embryogenesis. Development *137*, 3731-3742.

55. Green, S.A., Norris, R.P., Terasaki, M., and Lowe, C.J. (2013). FGF signaling induces mesoderm in the hemichordate *Saccoglossus kowalevskii*. Development *140*, 1024-1033.

56. McGregor, A.P., Pechmann, M., Schwager, E.E., and Damen, W.G. (2009). An ancestral regulatory network for posterior development in arthropods. Commun Integr Biol *2*, 174-176.

57. Martin, B.L., and Kimelman, D. (2009). Wnt signaling and the evolution of embryonic posterior development. Curr Biol *19*, R215-219.

58. Fritzenwanker, J.H., Uhlinger, K.R., Gerhart, J., Silva, E., and Lowe, C.J. (2019). Untangling posterior growth and segmentation by analyzing mechanisms of axis elongation in hemichordates. Proc Natl Acad Sci U S A *116*, 8403-8408.

59. Dictus, W.J.A.G., and Damen, P. (1997). Cell-lineage and clonal-contribution map of the trochophore larva of *Patella vulgata* (Mollusca). Mechanisms of Development *62*, 213-226.

60. Lyons, D.C., Perry, K.J., and Henry, J.Q. (2015). Spiralian gastrulation: germ layer formation, morphogenesis, and fate of the blastopore in the slipper snail *Crepidula fornicata*. Evodevo *6*, 24.

61. Koren, S., Walenz, B.P., Berlin, K., Miller, J.R., Bergman, N.H., and Phillippy, A.M. (2017). Canu: scalable and accurate long-read assembly via adaptive k-mer weighting and repeat separation. Genome Res *27*, 722-736.

62. Roach, M.J., Schmidt, S.A., and Borneman, A.R. (2018). Purge Haplotigs: allelic contig reassignment for third-gen diploid genome assemblies. BMC Bioinformatics *19*, 460.

63. Dobin, A., Davis, C.A., Schlesinger, F., Drenkow, J., Zaleski, C., Jha, S., Batut, P., Chaisson, M., and Gingeras, T.R. (2013). STAR: ultrafast universal RNA-seq aligner. Bioinformatics *29*, 15-21.

64. Venturini, L., Caim, S., Kaithakottil, G.G., Mapleson, D.L., and Swarbreck, D. (2018). Leveraging multiple transcriptome assembly methods for improved gene structure annotation. Gigascience *7*.

65. Stanke, M., Schoffmann, O., Morgenstern, B., and Waack, S. (2006). Gene prediction in eukaryotes with a generalized hidden Markov model that uses hints from external sources. BMC Bioinformatics *7*, 62.

66. Haas, B.J., Delcher, A.L., Mount, S.M., Wortman, J.R., Smith, R.K., Jr., Hannick, L.I., Maiti, R., Ronning, C.M., Rusch, D.B., Town, C.D., et al. (2003). Improving the *Arabidopsis* genome annotation using maximal transcript alignment assemblies. Nucleic Acids Res *31*, 5654-5666.

67. Seppey, M., Manni, M., and Zdobnov, E.M. (2019). BUSCO: Assessing Genome Assembly and Annotation Completeness. Methods Mol Biol *1962*, 227-245.

68. Bryant, D.M., Johnson, K., DiTommaso, T., Tickle, T., Couger, M.B., Payzin-Dogru, D., Lee, T.J., Leigh, N.D., Kuo, T.H., Davis, F.G., et al. (2017). A Tissue-Mapped Axolotl De Novo Transcriptome Enables Identification of Limb Regeneration Factors. Cell Rep *18*, 762-776.

69. Thomas, P.D., Campbell, M.J., Kejariwal, A., Mi, H., Karlak, B., Daverman, R., Diemer, K., Muruganujan, A., and Narechania, A. (2003). PANTHER: a library of protein families and subfamilies indexed by function. Genome Res *13*, 2129-2141.

70. Corces, M.R., Trevino, A.E., Hamilton, E.G., Greenside, P.G., Sinnott-Armstrong, N.A., Vesuna, S., Satpathy, A.T., Rubin, A.J., Montine, K.S., Wu, B., et al. (2017). An

improved ATAC-seq protocol reduces background and enables interrogation of frozen tissues. Nat Methods *14*, 959-962.

71. Picelli, S., Bjorklund, A.K., Reinius, B., Sagasser, S., Winberg, G., and Sandberg, R. (2014). Tn5 transposase and tagmentation procedures for massively scaled sequencing projects. Genome Res *24*, 2033-2040.

72. Martin, M. (2011). Cutadapt removes adapter sequences from high-throughput sequencing reads. 2011 *17*, 3.

73. Sedlazeck, F.J., Rescheneder, P., and von Haeseler, A. (2013). NextGenMap: fast and accurate read mapping in highly polymorphic genomes. Bioinformatics *29*, 2790-2791.

74. Li, H., Handsaker, B., Wysoker, A., Fennell, T., Ruan, J., Homer, N., Marth, G., Abecasis, G., Durbin, R., and Genome Project Data Processing, S. (2009). The Sequence Alignment/Map format and SAMtools. Bioinformatics *25*, 2078-2079.

75. Ramirez, F., Ryan, D.P., Gruning, B., Bhardwaj, V., Kilpert, F., Richter, A.S., Heyne, S., Dundar, F., and Manke, T. (2016). deepTools2: a next generation web server for deep-sequencing data analysis. Nucleic Acids Res *44*, W160-165.

76. Gaspar, J.M. (2018). Improved peak-calling with MACS2. bioRxiv, 496521.

77. Zhang, Y., Liu, T., Meyer, C.A., Eeckhoute, J., Johnson, D.S., Bernstein, B.E., Nusbaum, C., Myers, R.M., Brown, M., Li, W., et al. (2008). Model-based analysis of ChIP-Seq (MACS). Genome Biol *9*, R137.

78. Li, Q., Brown, J.B., Huang, H., and Bickel, P.J. (2011). Measuring reproducibility of high-throughput experiments. The Annals of Applied Statistics *5*, 1752-1779, 1728.

79. Heinz, S., Benner, C., Spann, N., Bertolino, E., Lin, Y.C., Laslo, P., Cheng, J.X., Murre, C., Singh, H., and Glass, C.K. (2010). Simple combinations of lineage-

determining transcription factors prime cis-regulatory elements required for macrophage and B cell identities. Mol Cell *38*, 576-589.

80. Bentsen, M., Goymann, P., Schultheis, H., Klee, K., Petrova, A., Wiegandt, R., Fust, A., Preussner, J., Kuenne, C., Braun, T., et al. (2020). ATAC-seq footprinting unravels kinetics of transcription factor binding during zygotic genome activation. Nat Commun *11*, 4267.

81. Quinlan, A.R., and Hall, I.M. (2010). BEDTools: a flexible suite of utilities for comparing genomic features. Bioinformatics *26*, 841-842.

82. Lopez-Delisle, L., Rabbani, L., Wolff, J., Bhardwaj, V., Backofen, R., Gruning, B., Ramirez, F., and Manke, T. (2021). pyGenomeTracks: reproducible plots for multivariate genomic datasets. Bioinformatics *37*, 422-423.

83. Bolger, A.M., Lohse, M., and Usadel, B. (2014). Trimmomatic: a flexible trimmer for Illumina sequence data. Bioinformatics *30*, 2114-2120.

84. Bray, N.L., Pimentel, H., Melsted, P., and Pachter, L. (2016). Near-optimal probabilistic RNA-seq quantification. Nat Biotechnol *34*, 525-527.

85. Love, M.I., Huber, W., and Anders, S. (2014). Moderated estimation of fold change and dispersion for RNA-seq data with DESeq2. Genome Biol *15*, 550.

86. Benjamini, Y., and Hochberg, Y. (1995). Controlling the False Discovery Rate: A Practical and Powerful Approach to Multiple Testing. Journal of the Royal Statistical Society. Series B (Methodological) *57*, 289-300.

87. Wickham, H. (2016). ggplot2: Elegant Graphics for Data Analysis, (Springer-Verlag New York).

88. Young, M.D., Wakefield, M.J., Smyth, G.K., and Oshlack, A. (2010). Gene ontology analysis for RNA-seq: accounting for selection bias. Genome Biol *11*, R14.

89. Kanehisa, M., Sato, Y., Kawashima, M., Furumichi, M., and Tanabe, M. (2016). KEGG as a reference resource for gene and protein annotation. Nucleic Acids Res *44*, D457-462.

90. UniProt, C. (2021). UniProt: the universal protein knowledgebase in 2021. Nucleic Acids Res *49*, D480-D489.

91. Katoh, K., Rozewicki, J., and Yamada, K.D. (2019). MAFFT online service: multiple sequence alignment, interactive sequence choice and visualization. Brief Bioinform *20*, 1160-1166.

92. Talavera, G., and Castresana, J. (2007). Improvement of phylogenies after removing divergent and ambiguously aligned blocks from protein sequence alignments. Syst Biol *56*, 564-577.

93. Stamatakis, A. (2014). RAxML version 8: a tool for phylogenetic analysis and post-analysis of large phylogenies. Bioinformatics *30*, 1312-1313.

94. Price, M.N., Dehal, P.S., and Arkin, A.P. (2010). FastTree 2--approximately maximum-likelihood trees for large alignments. PLoS One *5*, e9490.

95. Jones, P., Binns, D., Chang, H.Y., Fraser, M., Li, W., McAnulla, C., McWilliam, H., Maslen, J., Mitchell, A., Nuka, G., et al. (2014). InterProScan 5: genome-scale protein function classification. Bioinformatics *30*, 1236-1240.

Figures

Figure 1. Di-phosphorylated ERK1/2 is enriched in the 4d cell in *O. fusiformis*. (**A**) Spiralia is a major bilaterian lineage exhibiting spiral cleavage as the most probably synapomorphy. Differently from other bilaterian lineages, body patterning and embryonic organisation is controlled by a cell in the D-quadrant, which in molluscs exhibits and requires active di-phosphorilated ERK1/2. Whether the molluscan condition is ancestral to Spiralia is unclear. (**B**) *O. fusiformis* is a member of Palaeoannelida, the sister group to all remaining annelids, and undergoes typical equal spiral cleavage (**C**). The transition from the 4-cell to the 8-cell stage is characterised by a dextral shift of the mitotic spindle at a 45° angle relative to the animal–vegetal axis and generates a quartet of slightly larger animal cells (the micromeres, 1q) and a quartet of vegetal cells (the macromeres, 1Q). (**D**) Active di-phosporylated-ERK1/2 (yellow) is enriched in four animal cells ($1q^{111}$) at 4 hours post fertilisation (hpf), in a single cell (the 4d micromere) at 5hpf, and in six cells of the 2a-c lineage and 4d at 6 hpf. DAPI: cyan. (**E**) Dynamics of cleavage and quadrant identities during the onset and early division of 4d. The fourth micromere quartet emerges asymmetrically (early 4 hpf), which is soon followed by the asymmetric division of one of the 3q micromeres (arrowheads) (late 4 hpf). The vegetal pole is however quatri-radial at 5 hpf, with the 4d arresting its division with respect to 4a–c, and only cleaving into MR and ML after ingression at 7 hpf. F-actin (grey) shows cell boundaries and DAPI stains the nuclei. False colouring indicates cell or quadrant identities. Asterisks in (**C**) and (**D**) point to the animal pole, and to part of the 4d progeny in (**E**). Descriptions for (**D**) and (**E**) are based on at least 10 embryos per stage, except at 7 hpf (n = 3). Drawings are not to scale. Scale bars are 50 μm.

Figure 2. ERK1/2 signalling controls axial polarity in *O. fusiformis*. (**A**) ERK1/2 signalling cascade responds to cell-cell communication and involves the di-phosphorylation

of ERK1/2 (di-P-ERK1/2) via MEK. Brefeldin A (BFA), a protein trafficking inhibitor, and U0126, a specific MEK inhibitor, can block ERK1/2 di-phosphorylation. (**B**) Immunostaining against di-P-ERK1/2. BFA and U0126 treatments from 0.5 hours post fertilisation (hpf) to 5 hpf prevent di-P-ERK1/2 enrichment in the 4d cell at 5 hpf. (**C**) BFA and U0126 treatment (0.5 hpf to 5 hpf) result in anteroventrally radialised larvae that fail to form posterior structures (e.g., hindgut, mesodermal bands and chaetae). Main panels are lateral z-stack projections of confocal images and insets in treated embryos are ventral views. Cilia is labelled with anti-acetylated tubulin. (**D**) Whole mount *in situ* hybridisation on control and U0126 treated (0.5 to 5 hpf) larvae. Treated radial larvae show reduced apical markers (*six3/6*, and *syt-1* in the inset), radially expanded anterior markers (*gsc*), and absent posterior endomesodermal (*cdx*, *twist*) but not a midgut gene (GATA4/5/6b). (**E**) Schematic representation of drug treatment windows and observed larval phenotypes (WT, wild type; R, radial). (**F**) Morphological analysis of the compressed larval phenotype obtained after BFA treatment from 0.5 hpf until 3–4 hpf. Treated larvae have a reduced apical organ and apical tuft (first row) and reduced expression of apical gene markers (*six3/6*, and *syt-1* in the inset), but other tissues are not affected. The larval blastocele is somehow obliterated. Asterisks point to the apical pole. Schematic drawings are not to scale. ao: apical organ; an: anus; ch: chaetae; mg: midgut; mo: mouth; pt: prototroch. Scale bars are 50 μm.

Figure 3. ERK1/2 signalling activates posterodorsal and mesodermal genes. (**A**) Experimental design for RNA-seq collections. Solid colour bars show period of control (DMSO), BFA or U0126 treatments. Red circles show sample collection, at the coeloblastula stage (5.5 hpf) and at the larval stage (24 hpf). (**B**) Number of differentially expressed (DE) genes in different conditions and comparisons, where red bars are downregulated genes and blue bars are upregulated genes. (**C**) Volcano plots for BFA and U0126 treated coeloblastula.

Red dots show DE genes, with candidate genes labelled for each comparison. (**D**) Temporal and spatial time course of expression of candidate genes affected by 4d misspecification and associated with apical/anterior, chaetae/posterior, hindgut or mesoderm development. The heatmap depicts the normalised z-score value of expression for each gene throughout development, with red blocks indicating high levels of expression and blue blocks indicating low levels of expression. The horizontal dotted line highlights the timing of 4d specification. On the right, whole mount *in situ* hybridisation of a subset of these 22 candidate genes at the coeloblastula (5 hpf), gastrula (9 hpf) and larval stages (24 hpf). (**E**) Only three of the candidate genes (*cdx*, *foxH* and *fer3*) are downregulated in all stages and treatment comparisons. Validation via *in situ* hybridisation demonstrates the expression is lost after drug treatment. Pictures for *cdx* at the coeloblastula and larva in (**D**) and (**E**) are the same. Asterisks point to the animal/apical pole, and arrowheads to the domains of expression. Schematic drawings are not to scale. bp: blastopore; mo: mouth.

Figure 4. ERK1/2 signalling specifies and patterns the D-quadrant. (**A**) Whole mount *in situ* hybridisation of a subset of genes (ERK1/2-dependent and independent) patterning the vegetal pole at (5 hpf) and after (5.5 hpf) 4d specification. The row below is a schematic representation of the vegetal pole depicting gene expression (in green) at 5.5 hpf. (**B**) The ParaHox gene *cdx* (yellow) is expressed in the 4d cell at the coeloblastula stage and in the progeny of MR and ML at the gastrula stage, corroborating the endodermal sublineage of 4d. (**C**) The Notch ligand *delta* (yellow) is expressed in 4d, multiple cells from the D-quadrant, and a few animal micromeres from the other three quadrants at the coeloblastula stage. In (**B**, **C**) Nuclei (DAPI) are shown in cyan and cell boundaries (acetylated tubulin) in magenta. Asterisks point to the animal pole. (**D**) Distribution of known bound transcription factors in open chromatin regions around *cdx* (upper part) and *delta* (lower part) loci at 5 hpf. Dark and

light blue depict the two ATAC-seq replicates. (**E**) Number of cellular contacts for each of the 4q micromeres at 5.5 hpf based on the analysis of eight embryos. While $4a^1$–$4c^2$ establish 8 direct cell contacts, 4d touches 13 cells of the D and C quadrants. (**F**) Inhibition of ERK1/2 di-phosphorylation by U0126 prevents D-quadrant specification, as shown by the expansion of the anterior marker *gsc* and loss of the posterior marker *AP2*. The 4d micromere is no longer recognised, as all 4q micromeres cleave at the same time (asterisks). However, *gsc* is lost in BFA treated embryos, and thus needs of inductive signals. Gene expression is shown in yellow, nuclei (DAPI) in cyan and cell boundaries (acetylated tubulin) in magenta or grey. In all panels, arrowheads point to expression domains. Schematic drawings are not to scale. gp: gastral plate.

Figure 5. FGFR signalling regulates ERK1/2 di-phosphorylation in 4d. (**A**) The drug SU5402 specifically inhibits receptors tyrosine kinase of the type FGF/VEGF, which can signal through the ERK1/2 signalling cascade. (**B**) Whole mount immunohistochemistry against di-phosphorylated ERK1/2 (di-P-ERK1/2). SU5402 treated embryos lose ERK1/2 enrichment in a vegetal micromere at 5 hours post fertilisation (hpf). (**C**) Schematic representation of drug treatment windows and observed larval phenotypes (WT, wild type). (**D**) Morphological and molecular patterning analysis of SU5402 treated embryos (4 to 6 hpf) fixed at 24 hpf. The first column shows diagrams of lateral views of the wild type in DMSO controls and radial larvae in treated embryos. Second and third columns show larvae labelled with DAPI (cyan) and F-actin (magenta) plus acetylated tubulin staining (yellow), respectively. Fourth column onwards are whole mount in situ hybridisations. SU5402 treatment from 4 hpf to 6 hpf results in phenocopies of U0126 and BFA radial larvae. Insets are ventral views. Asterisks point to the apical pole. Schematic drawings are not to scale. ao: apical organ; an: anus; ch: chaetae; mg: midgut; mo: mouth; pt: prototroch.

Figure 6. ERK1/2 activity in the D-quadrant embryonic organiser is an ancestral spiralian trait. (**A**) Schematic model of FGFR/ERK1/2 activity in the 4d micromere during late spiral cleavage in *O. fusiformis*. At 4 hours post fertilisation (hpf), di-phosphorylated ERK1/2 (di-P-ERK1/2) is enriched in the apical most micromeres ($1q^{111}$). At 5 hpf, an unidentified signal activates FGF receptor (FGFR) which di-phosphorylates ERK1/2 in the 4d micromere. This activates *cdx* and *delta* in 4d (becoming the endomesodermal precursor) and correlates with 4d arresting its cell cycle progression, as 4a–4c cleave. ERK1/2 activation in 4d is required to limit an anteriorising signal (Signal X) to the A–C quadrants, which activates *gsc* expression in these quadrants. In addition, ERK1/2 activity in 4d induces the expression of a battery of genes in the D-quadrant and part of the C-quadrant that probably induce lateral mesodermal and posterodorsal fates, ultimately controlling axial elongation. This inductive activity might happen via the Notch pathway. (**B**) The similarities in ERK1/2 activation patterns between *O. fusiformis* and other molluscan embryos suggest this is a shared ancestral trait to spiral cleavage. More broadly, ERK1/2 activity induces the expression of a set of genes and signalling pathways that are repeatedly involved in posterior specification and anteroposterior growth in bilaterian embryos. Drawings are not to scale.

Supplemental Information

Figure S1. ERK1/2 activity during *O. fusiformis* early embryogenesis. (**A**) Maximum likelihood orthology assignment for ERK1/2, using ERK5 as outgroup. Only bootstrap values for major nodes are shown. (**B**) DEseq2 normalised expression of *erk1/2* during *O. fusiformis* development, from the active oocyte to the mitraria larval stage. The time of the specification of 4d is highlighted with a schematic drawing. Coloured dots indicate values of expression for each replicate and the dotted red line shows the mean value of expression. (**C**) Whole mount immunohistochemistry against di-phosphorylated-ERK1/2 (dark orange) during spiral cleavage in *O. fusiformis*. ERK1/2 is active at low levels during early divisions, and later enriched in the four $1q^{111}$ animal micromeres at 4 hours post fertilisation (hpf), the 4d micromere at the time of its specification (5 hpf) and finally in six vegetal cells forming a bilaterally symmetrical pattern (arrowheads) at 6 hpf. Insets in (**C**) show either nuclear staining (blue) or lateral views. Asterisks point to the animal pole.

Figure S2. The effect of BFA and U0126 treatment in *O. fusiformis* development. (**A**) Percentage of coeloblastula showing di-phosphorylated ERK1/2 (di-P-ERK1/2) enrichment in the 4d micromere after 0.5 to 5 hours post fertilisation (hpf) treatment with brefeldin A (BFA), U0126 or DMSO (control). (**B**) Percentage of radial phenotypes obtained when treating embryos from 0.5 to 5 hpf with a range of BFA and U0126 concentrations. (**C**) Whole mount in situ hybridisation of apical (*six3/6*), oral (*gsc*), posterior/hindgut (*cdx*), midgut (*GATA4/5/6b*) and trunk mesodermal (*twist*) gene markers in control and treated larvae. Radial phenotypes have a reduction of the apical marker, radial expansion of an oral gene, loss of posterior structures (chaetae) and posterior/trunk mesoderm gene expression and retain the expression of a midgut gene. Radial larvae treated with U0126 from the 2-cell stage to 3 hpf show scattered *twist* expression in some embryos (arrowheads). The compressed

larval phenotype after BFA treatment from 0.5 to 4 hpf have a reduced apical organ and apical tuft (first row) and reduced expression of apical markers (*six3/6*), but otherwise normal morphology besides an obliterated internal blastocele. Asterisks indicate the apical pole and arrowheads point to expression domains. Insets are ventral views. mo: mouth.

Figure S3. Differential expression analyses in BFA and U0126 treated embryos. (**A**) Hierarchical pairwise correlation matrix between brefeldin A (BFA) and U0126 treated and control samples. (**B**) Principal component analysis (PCA) plot for BFA (left) and U0126 (right) RNA-seq analyses. (**C**) Volcano plots for BFA and U0126 treated larva. Red dots show differentially expressed (DE) genes and analysed candidate genes are labelled in each comparison. (**D**) Venn diagrams showing the number of up- (top) and downregulated (bottom) DE genes shared between different conditions. (**E**) Ten most overrepresented KEGG pathways in each of the four conditions analysed by RNA-seq. The size of the coloured dots is proportional to the number of overrepresented sub-categories nested into a given KEGG pathway.

Figure S4. Validation of the differential expression analyses. (**A**–**G**) Whole mount in situ hybridisation of control and treated embryos showing in addition a wild type gastrula stage to reconstruct the time course of expression of each gene. In all cases, the expression patterns disappear in BFA and U0126 treated embryos. Insets are ventral views. Asterisk point to the animal/apical pole. Arrowheads point to 4d in (**A**) and to the apical organ in (**F**). bp: blastopore; gp: gastral plate; mo: mouth.

Figure S5. Genes patterning the D-quadrant after the specification of the 4d-organiser cell. (**A**) Schematic drawing of the cellular arrangements and cell nomenclature of the vegetal

pole just after the specification of the 4d micromere in *O. fusiformis* embryo at 5.5 hours post fertilisation (hpf). Different colours depict different quadrants. (**B**) Time course of expression of *cdx*, *foxH* and *fer3* via whole mount *in situ* hybridisation from 6 hpf to 18 hpf during *O. fusiformis* embryogenesis. While *cdx* is expressed in the cells forming the hindgut, *foxH* appears to upregulate at the earliest stages of cells giving rise to mesodermal derivatives. The gene *fer3* is expressed in two posterior most cells of unknown function in the gastrula and larva. Insets are lateral views. (**C**) The protein domain architecture of the Notch ligand DELTA in *O. fusiformis* in comparisons with the domain structures of the Delta orthologs in *D. melanogaster* and *H. sapiens*. (**D–G**) Maximum likelihood orthology assignments of DELTA, FOXH, WNT ligands, and RHOX in *O. fusiformis*. Only bootstrap values supporting each major clade are shown. bp: blastopore; mo: mouth.

Figure S6. The FGF pathway and FGFR activity during 4d specification in *O. fusiformis*. (**A**) Maximum likelihood orthology assignment of fibroblast growth factor receptor (FGFR) and vascular endothelial growth factor receptor (VEGFR). Only bootstrap values for key nodes are shown. (**B**) Multiple protein alignment between *O. fusiformis* and *H. sapiens* FGFR and VEGFR orthologs indicating conserved residues for the interaction of the drug SU5402 with these receptors. (**C**) Temporal time course of expression of members of the FGF and VEGF pathways in *O. fusiformis*. The heatmap depicts the normalised z-score value of expression for each gene, with red blocks indicating high levels of expression and blue blocks indicating low levels of expression. The horizontal dotted line highlights the specification of the 4d micromere. (**D**) Whole mount in situ hybridisation for *FGFR* and *VEGFR* at the coeloblastula stage of *O. fusiformis*. *FGFR* is expressed weakly at the gastral plate at the time of 4d-instructed posterior re-pattering. (**E**) Proportion of treated and control embryos exhibiting di-phosphorylated ERK1/2 enrichment in the 4d cell at 5 hpf after

SU5402 drug treatment from 0.5 to 5 hours post fertilisation (hpf). (**F**) Morphological and molecular characterisation of SU5402 treated embryos fixed at the larval stage. The first column shows diagrams of lateral views of the wild type, compressed and radial phenotypes. From the second column onwards, whole mount *in situ* hybridisations of control and SU5402 treated larvae. The compressed larvae are phenocopies of brefeldin A (BFA) compressed larvae, with reduced apical organ and apical tuft (second row) and reduced expression of apical markers (*six3/6*), but other tissues are not affected. Radial larvae are phenocopies of BFA and U0126 radial larvae with reduction of apical markers (*six3/*6), radial expansion of oral genes (*gsc*), loss of posterior structures (chaetae) and expression of posterior endomesodermal markers (*cdx*, *twist*), but normal expression of an endodermal gene (*GATA4/5/6b*). Insets are ventral views. Asterisks point to the animal/apical pole. ao: apical organ; an: anus; ch: chaetae; gp: gastral plate; mg: midgut; mo: mouth; pt: prototroch. Scale bars are 50 μm.

Supplementary Tables and Files

Table S1. Di-P-ERK1/2 activation in spiralians.

Table S2. Di-P-ERK1/2 activation at 5 hpf in control, BFA and U0126 treated embryos.

Table S3. Larval phenotypes in control, BFA and U0126 treatments.

Table S4. Larval phenotypes at different concentrations of BFA and U0126.

Table S5. Larval phenotypes during staggered time windows of BFA and U0126 treatments.

Table S6. List of all differentially expressed genes at 5.5 hpf and 24 hpf.

Table S7. List of enriched gene ontology terms.

Table S8. List of enriched KEGG pathways.

Table S9. List of candidate genes and their gene IDs in differential gene expression analyses.

File S1. Multiple protein alignments

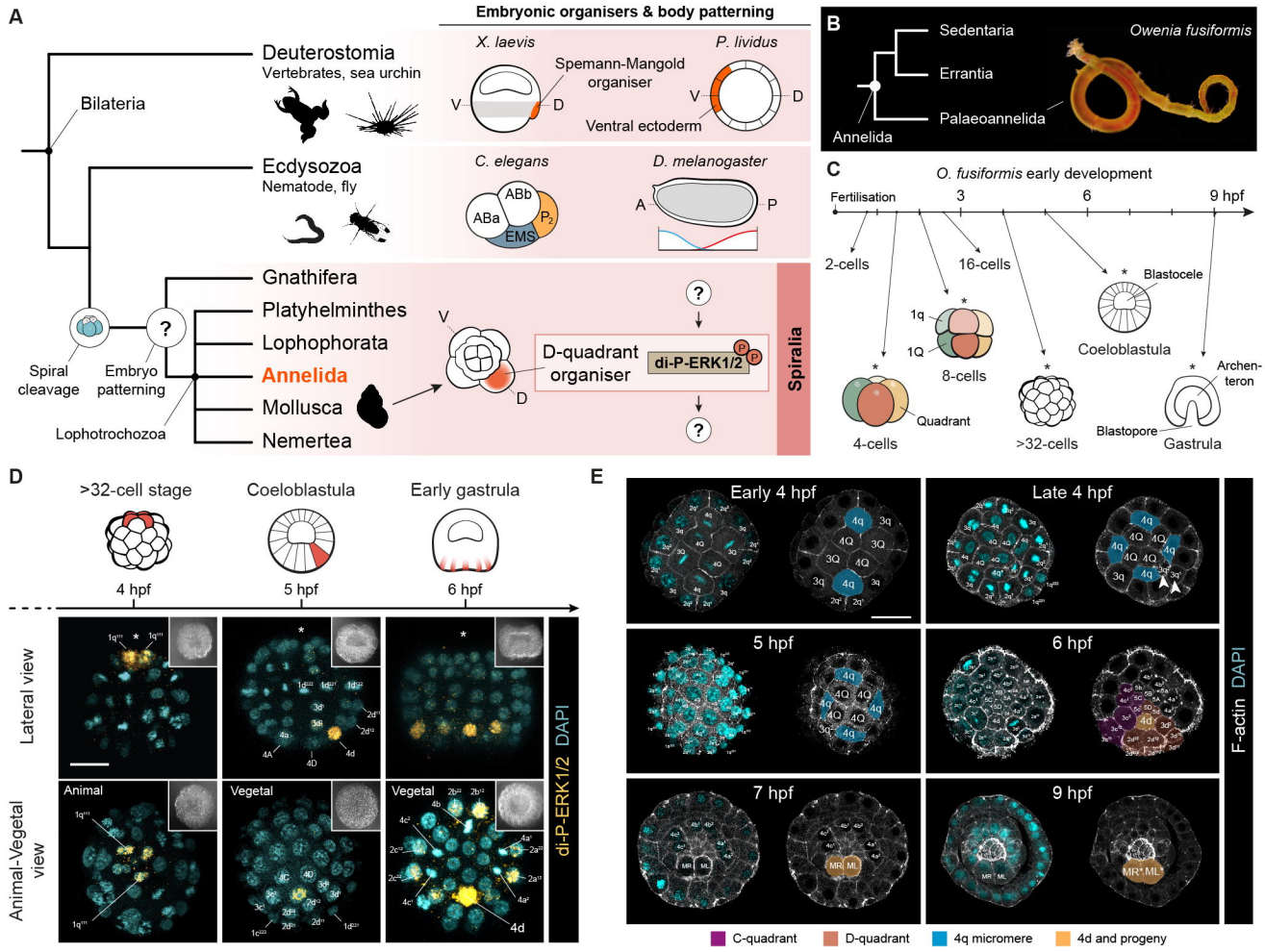
A
Embryonic organisers & body patterning
Deuterostomia
Vertebrates, sea urchin
Bilateria
X. laevis
Spemann-Mangold organiser
V
D
P. lividus
Ventral ectoderm
Ecdysozoa
Nematode, fly
C. elegans
ABb
ABa
P2
EMS
D. melanogaster
A
P
Gnathifera
Platyhelminthes
Lophophorata
Annelida
Mollusca
Nemertea
Spiral cleavage
Embryo patterning
Lophotrochozoa
D-quadrant organiser
di-P-ERK1/2
Spiralia
B
Sedentaria
Errantia
Palaeoannelida
Annelida
Owenia fusiformis
C
O. fusiformis early development
Fertilisation
3
6
9 hpf
2-cells
16-cells
Blastocele
1q
1Q
8-cells
Coeloblastula
Quadrant
4-cells
>32-cells
Blastopore
Archen-teron
Gastrula
D
>32-cell stage
Coeloblastula
Early gastrula
4 hpf
5 hpf
6 hpf
Lateral view
Animal-Vegetal view
Animal
Vegetal
di-P-ERK1/2 DAPI
E
Early 4 hpf
Late 4 hpf
5 hpf
6 hpf
7 hpf
9 hpf
F-actin DAPI
C-quadrant
D-quadrant
4q micromere
4d and progeny

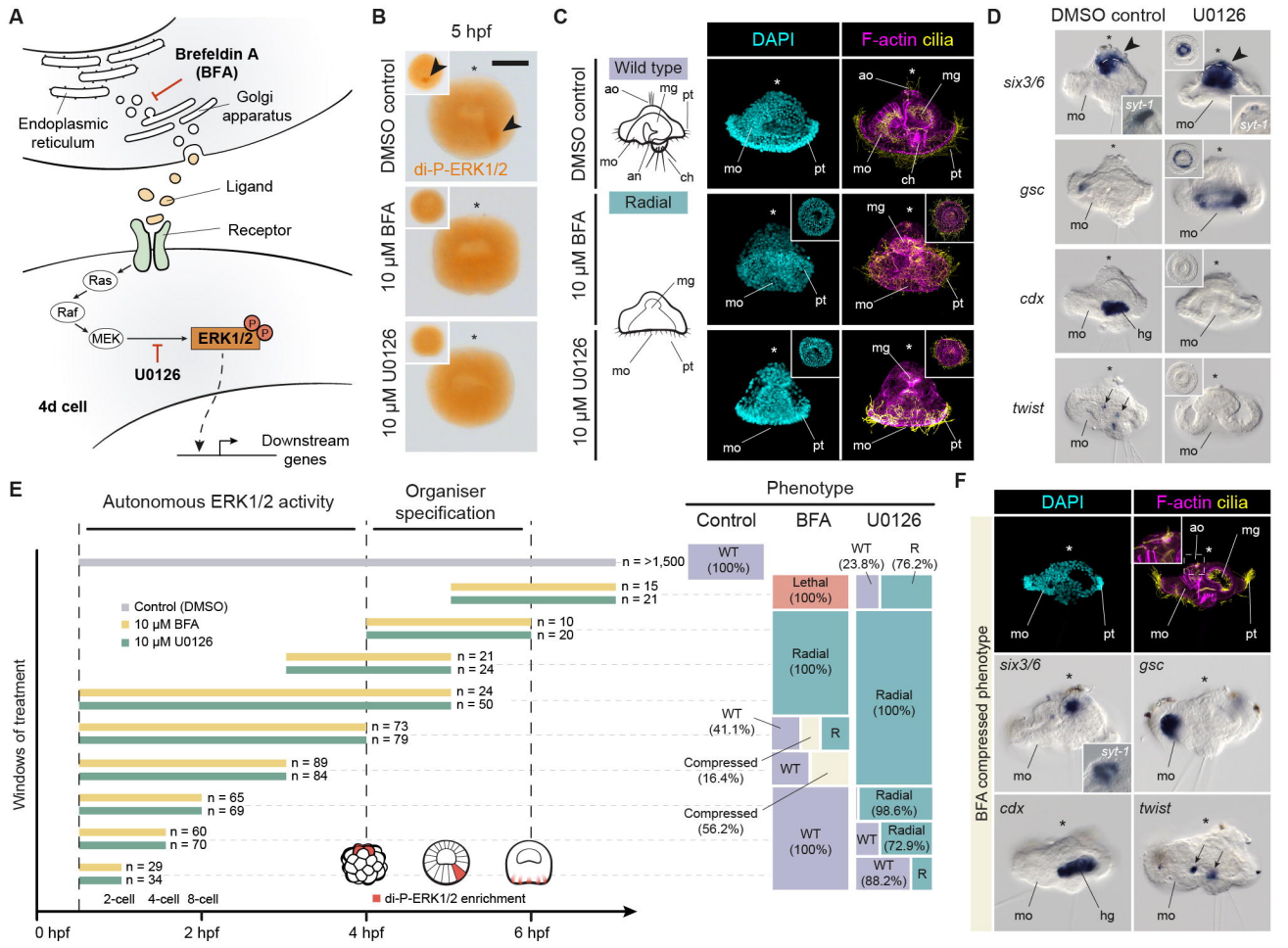
A
Brefeldin A (BFA)
Golgi apparatus
Endoplasmic reticulum
Ligand
Receptor
Ras
Raf
MEK
ERK1/2
U0126
4d cell
Downstream genes
B
5 hpf
DMSO control
10 µM BFA
10 µM U0126
di-P-ERK1/2
C
DAPI
F-actin cilia
Wild type
Radial
DMSO control
10 µM BFA
10 µM U0126
ao
mg
pt
mo
an
ch
D
DMSO control
U0126
six3/6
gsc
cdx
twist
syt-1
hg
E
Autonomous ERK1/2 activity
Organiser specification
Phenotype
Control
BFA
U0126
Windows of treatment
Control (DMSO)
10 µM BFA
10 µM U0126
n = >1,500
n = 15
n = 21
n = 10
n = 20
n = 21
n = 24
n = 24
n = 50
n = 73
n = 79
n = 89
n = 84
n = 65
n = 69
n = 60
n = 70
n = 29
n = 34
WT (100%)
Lethal (100%)
Radial (100%)
WT (41.1%)
R
Compressed (16.4%)
WT
Compressed (56.2%)
WT (100%)
WT (23.8%)
R (76.2%)
Radial (100%)
Radial (98.6%)
WT
Radial (72.9%)
WT (88.2%)
R
2-cell
4-cell
8-cell
di-P-ERK1/2 enrichment
0 hpf
2 hpf
4 hpf
6 hpf
F
DAPI
F-actin cilia
BFA compressed phenotype
six3/6
gsc
cdx
twist
syt-1
mo
hg

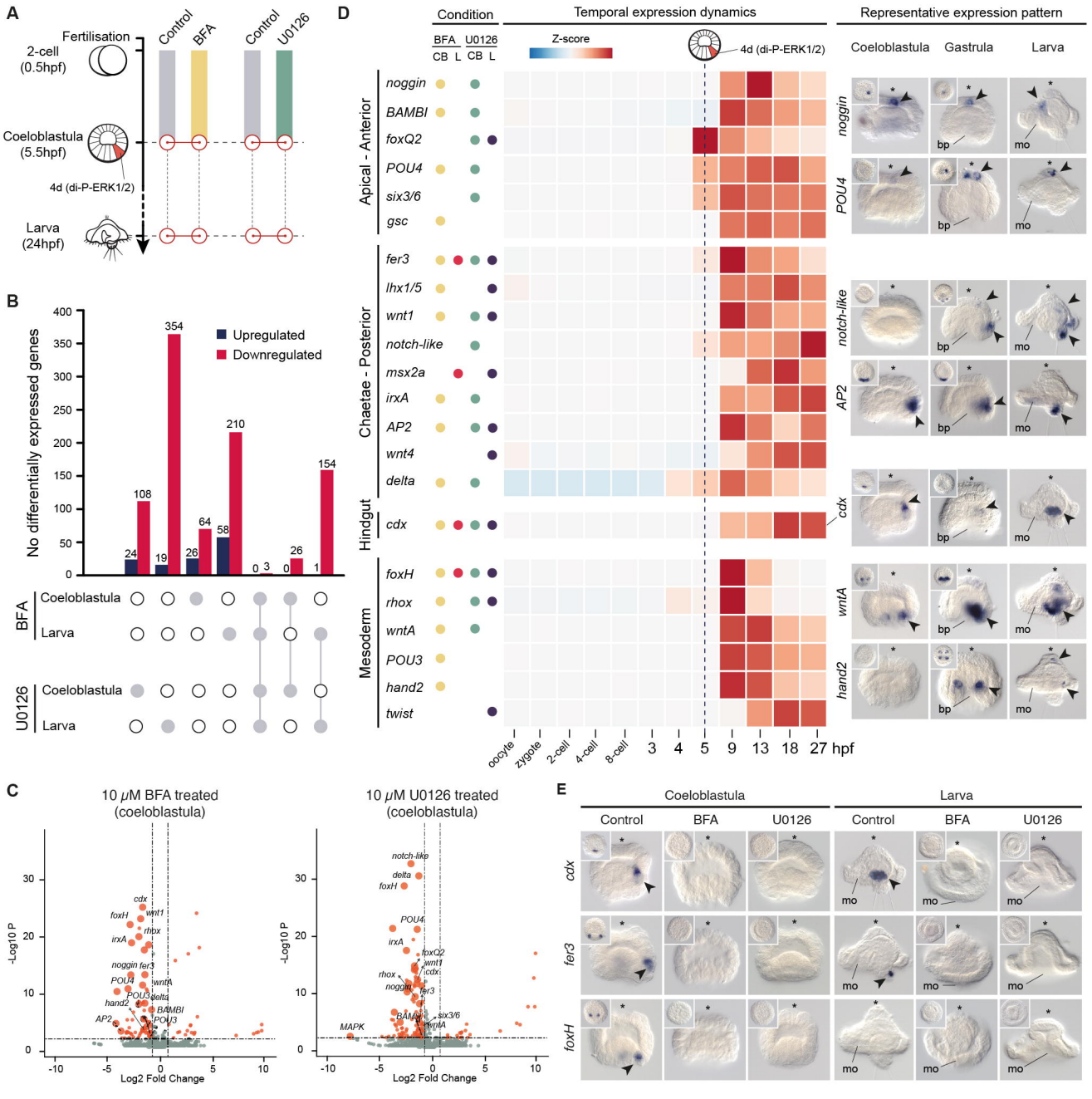
A
Fertilisation
2-cell (0.5hpf)
Coeloblastula (5.5hpf)
4d (di-P-ERK1/2)
Larva (24hpf)
Control
BFA
Control
U0126
B
No differentially expressed genes
Upregulated
Downregulated
BFA
Coeloblastula
Larva
U0126
Coeloblastula
Larva
C
10 μM BFA treated (coeloblastula)
10 μM U0126 treated (coeloblastula)
-Log10 P
Log2 Fold Change
D
Condition
BFA U0126
CB L CB L
Temporal expression dynamics
Z-score
4d (di-P-ERK1/2)
Representative expression pattern
Coeloblastula
Gastrula
Larva
Apical - Anterior
Chaetae - Posterior
Hindgut
Mesoderm
noggin
BAMBI
foxQ2
POU4
six3/6
gsc
fer3
lhx1/5
wnt1
notch-like
msx2a
irxA
AP2
wnt4
delta
cdx
foxH
rhox
wntA
POU3
hand2
twist
oocyte
zygote
2-cell
4-cell
8-cell
3
4
5
9
13
18
27 hpf
bp
mo
E
Coeloblastula
Larva
Control
BFA
U0126
cdx
fer3
foxH

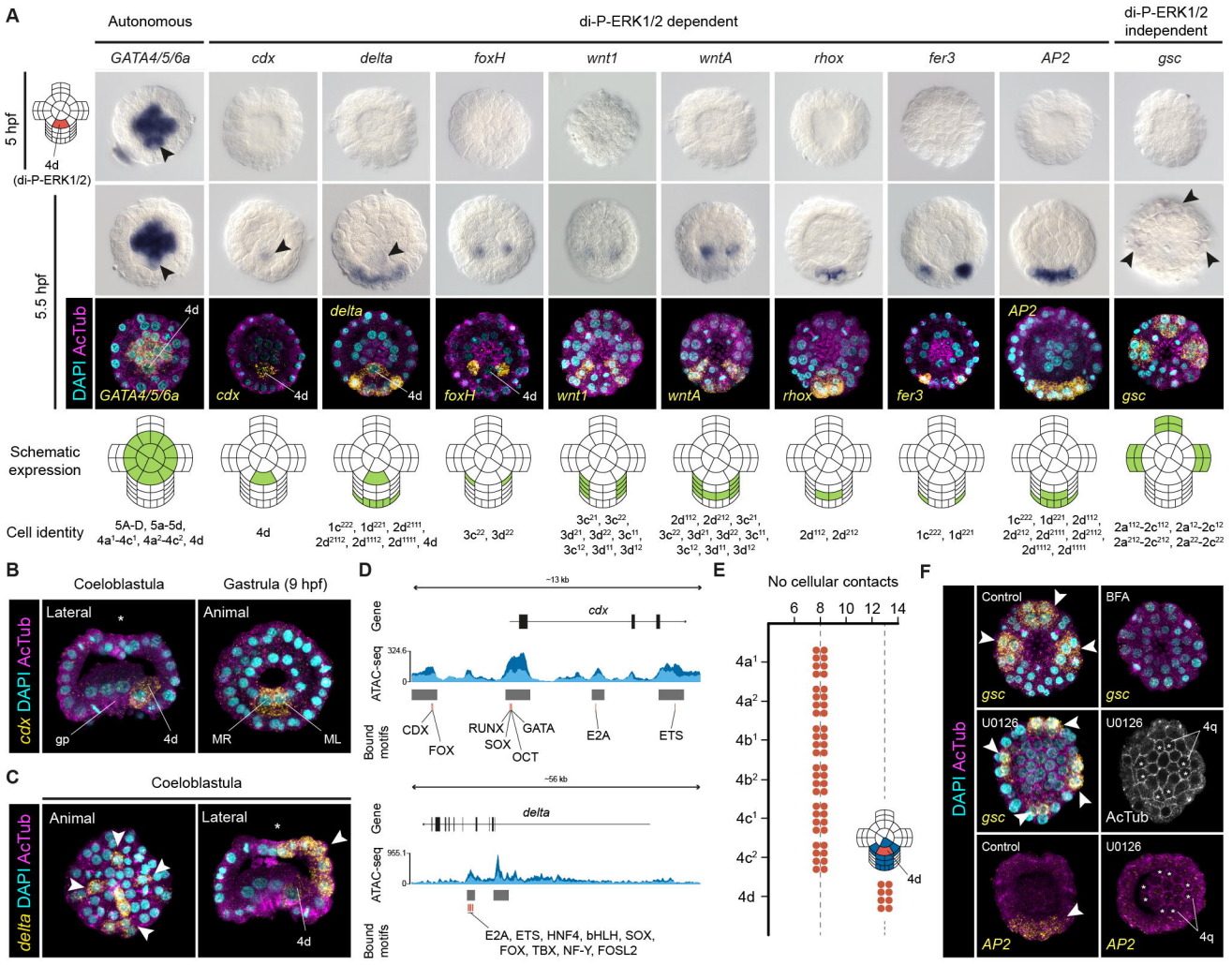
A
Autonomous
di-P-ERK1/2 dependent
di-P-ERK1/2 independent
GATA4/5/6a
cdx
delta
foxH
wnt1
wntA
rhox
fer3
AP2
gsc
5 hpf
4d
(di-P-ERK1/2)
5.5 hpf
DAPI AcTub
Schematic expression
Cell identity
5A-D, 5a-5d, 4a1-4c1, 4a2-4c2, 4d
4d
1c222, 1d221, 2d2111, 2d2112, 2d1112, 2d1111, 4d
3c22, 3d22
3c21, 3c22, 3d21, 3d22, 3c11, 3c12, 3d11, 3d12
2d112, 2d212, 3c21, 3c22, 3d21, 3d22, 3c11, 3c12, 3d11, 3d12
2d112, 2d212
1c222, 1d221
1c222, 1d221, 2d112, 2d212, 2d2111, 2d2112, 2d1112, 2d1111
2a112-2c112, 2a12-2c12, 2a212-2c212, 2a22-2c22
B
Coeloblastula
Gastrula (9 hpf)
Lateral
Animal
cdx DAPI AcTub
gp
MR
ML
C
Coeloblastula
Animal
Lateral
delta DAPI AcTub
D
~13 kb
Gene
cdx
ATAC-seq
324.6
Bound motifs
CDX
FOX
RUNX
SOX
GATA
OCT
E2A
ETS
~56 kb
delta
955.1
E2A, ETS, HNF4, bHLH, SOX, FOX, TBX, NF-Y, FOSL2
E
No cellular contacts
6
8
10
12
14
4a1
4a2
4b1
4b2
4c1
4c2
4d
F
Control
BFA
U0126
gsc
AP2
AcTub
4q
DAPI AcTub

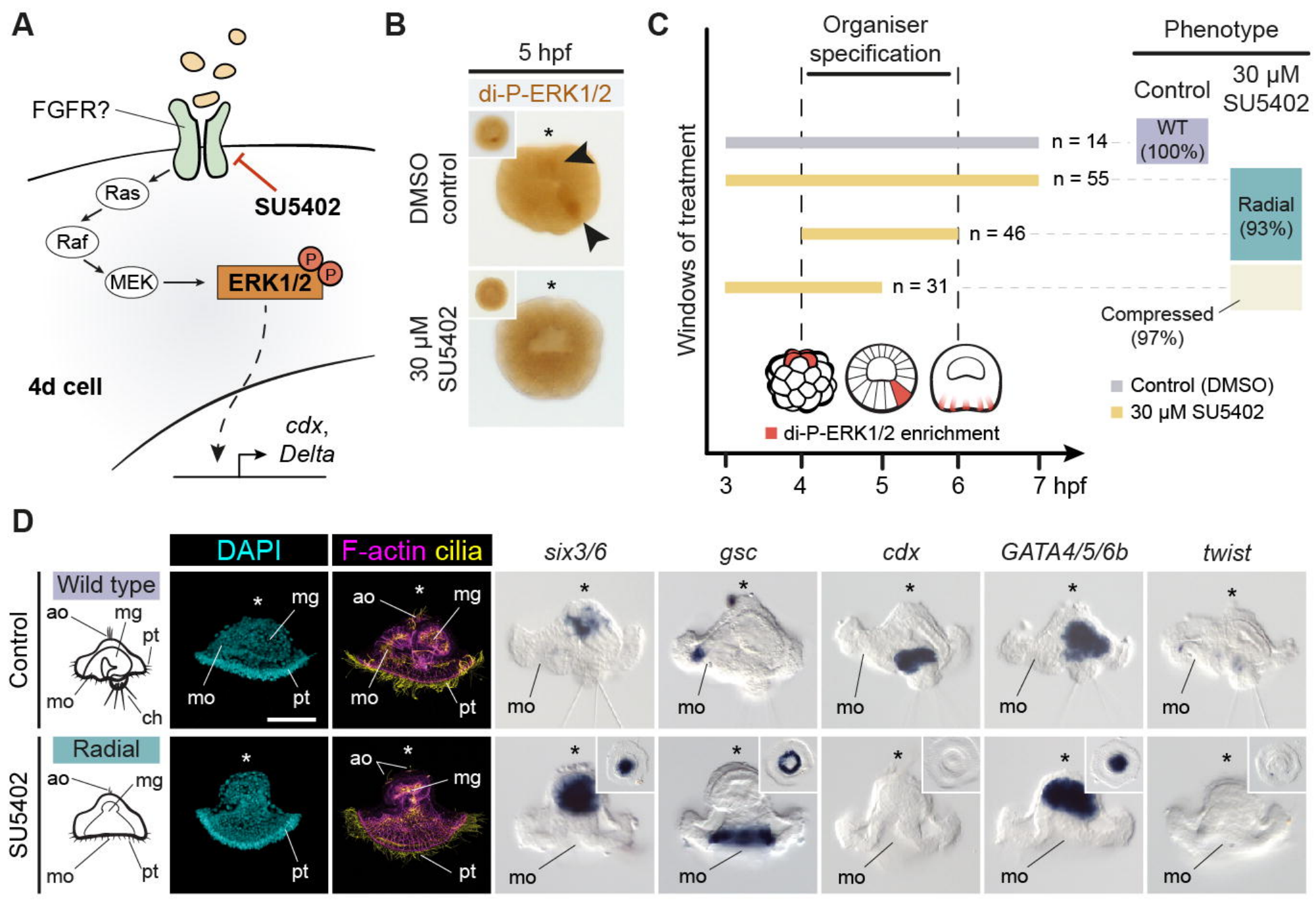
A
FGFR?
Ras
Raf
MEK
ERK1/2
P
P
SU5402
4d cell
cdx,
Delta
B
5 hpf
di-P-ERK1/2
DMSO control
30 µM SU5402
*
C
Organiser specification
Phenotype
Control
30 µM SU5402
Windows of treatment
n = 14
n = 55
n = 46
n = 31
WT (100%)
Radial (93%)
Compressed (97%)
Control (DMSO)
30 µM SU5402
di-P-ERK1/2 enrichment
3
4
5
6
7 hpf
D
DAPI
F-actin cilia
six3/6
gsc
cdx
GATA4/5/6b
twist
Wild type
Control
Radial
SU5402
ao
mg
pt
mo
ch
*

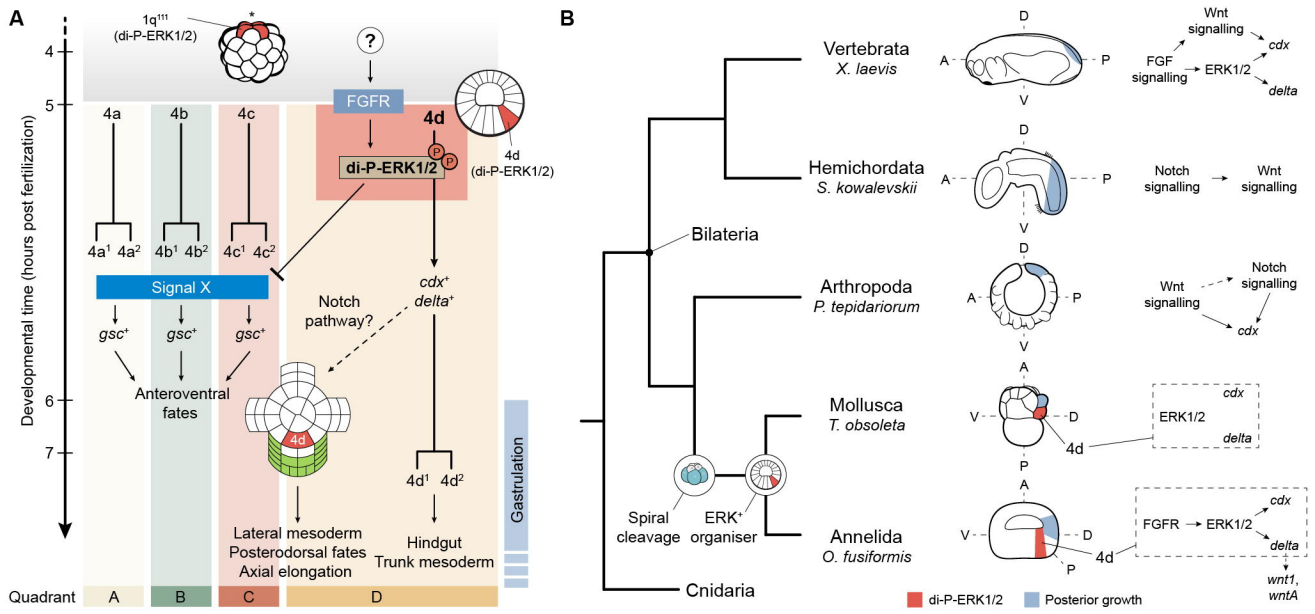
A
Developmental time (hours post fertilization)
4
5
6
7
1q111 (di-P-ERK1/2)
*
?
FGFR
4d
di-P-ERK1/2
P
P
4d (di-P-ERK1/2)
4a
4b
4c
4a1 4a2
4b1 4b2
4c1 4c2
Signal X
gsc+
gsc+
gsc+
Anteroventral fates
Notch pathway?
cdx+
delta+
4d
4d1 4d2
Lateral mesoderm
Posterodorsal fates
Axial elongation
Hindgut
Trunk mesoderm
Gastrulation
Quadrant
A
B
C
D
B
Vertebrata
X. laevis
D
A
P
V
Wnt signalling
FGF signalling
ERK1/2
cdx
delta
Hemichordata
S. kowalevskii
Notch signalling
Wnt signalling
Bilateria
Arthropoda
P. tepidariorum
Wnt signalling
Notch signalling
cdx
Mollusca
T. obsoleta
ERK1/2
cdx
delta
4d
Spiral cleavage
ERK+ organiser
Annelida
O. fusiformis
FGFR
ERK1/2
cdx
delta
wnt1, wntA
Cnidaria
di-P-ERK1/2
Posterior growth

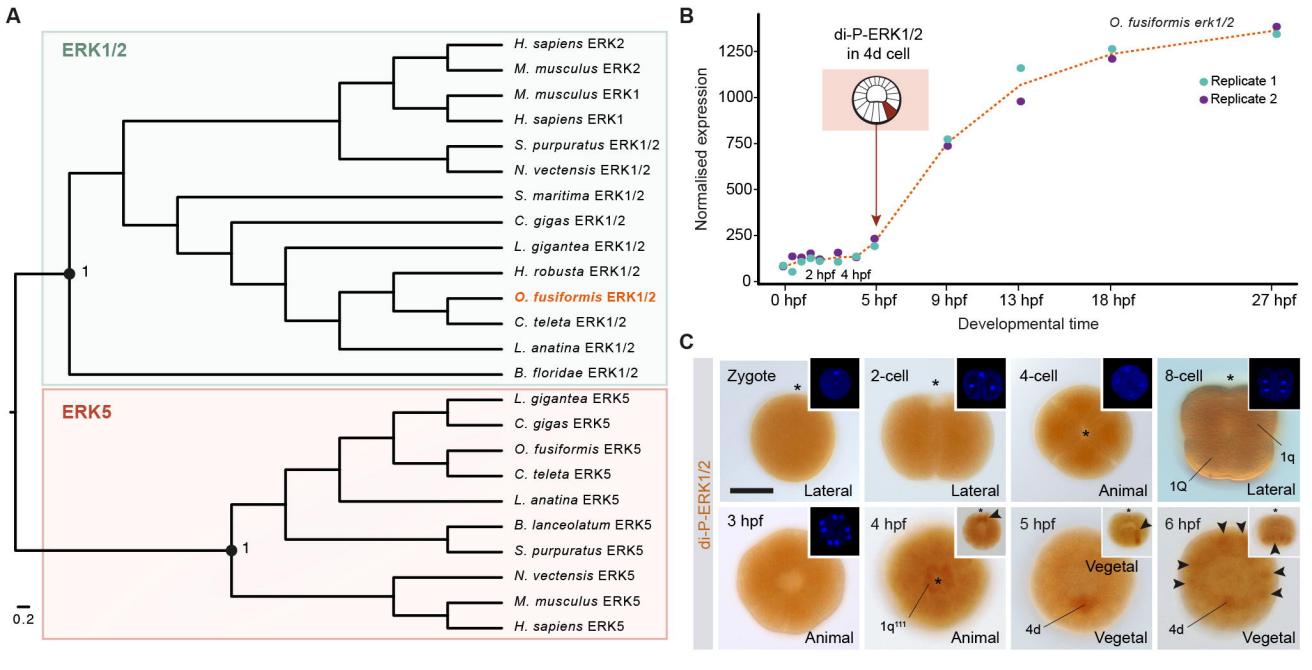
A
ERK1/2
H. sapiens ERK2
M. musculus ERK2
M. musculus ERK1
H. sapiens ERK1
S. purpuratus ERK1/2
N. vectensis ERK1/2
S. maritima ERK1/2
C. gigas ERK1/2
L. gigantea ERK1/2
H. robusta ERK1/2
O. fusiformis ERK1/2
C. teleta ERK1/2
L. anatina ERK1/2
B. floridae ERK1/2
1
ERK5
L. gigantea ERK5
C. gigas ERK5
O. fusiformis ERK5
C. teleta ERK5
L. anatina ERK5
B. lanceolatum ERK5
S. purpuratus ERK5
N. vectensis ERK5
M. musculus ERK5
H. sapiens ERK5
1
0.2
B
di-P-ERK1/2
in 4d cell
O. fusiformis erk1/2
Replicate 1
Replicate 2
Normalised expression
1250
1000
750
500
250
0
2 hpf 4 hpf
0 hpf
5 hpf
9 hpf
13 hpf
18 hpf
27 hpf
Developmental time
C
di-P-ERK1/2
Zygote
Lateral
2-cell
Lateral
4-cell
Animal
8-cell
1q
1Q
Lateral
3 hpf
Animal
4 hpf
1q111
Animal
5 hpf
Vegetal
4d
Vegetal
6 hpf
4d
Vegetal

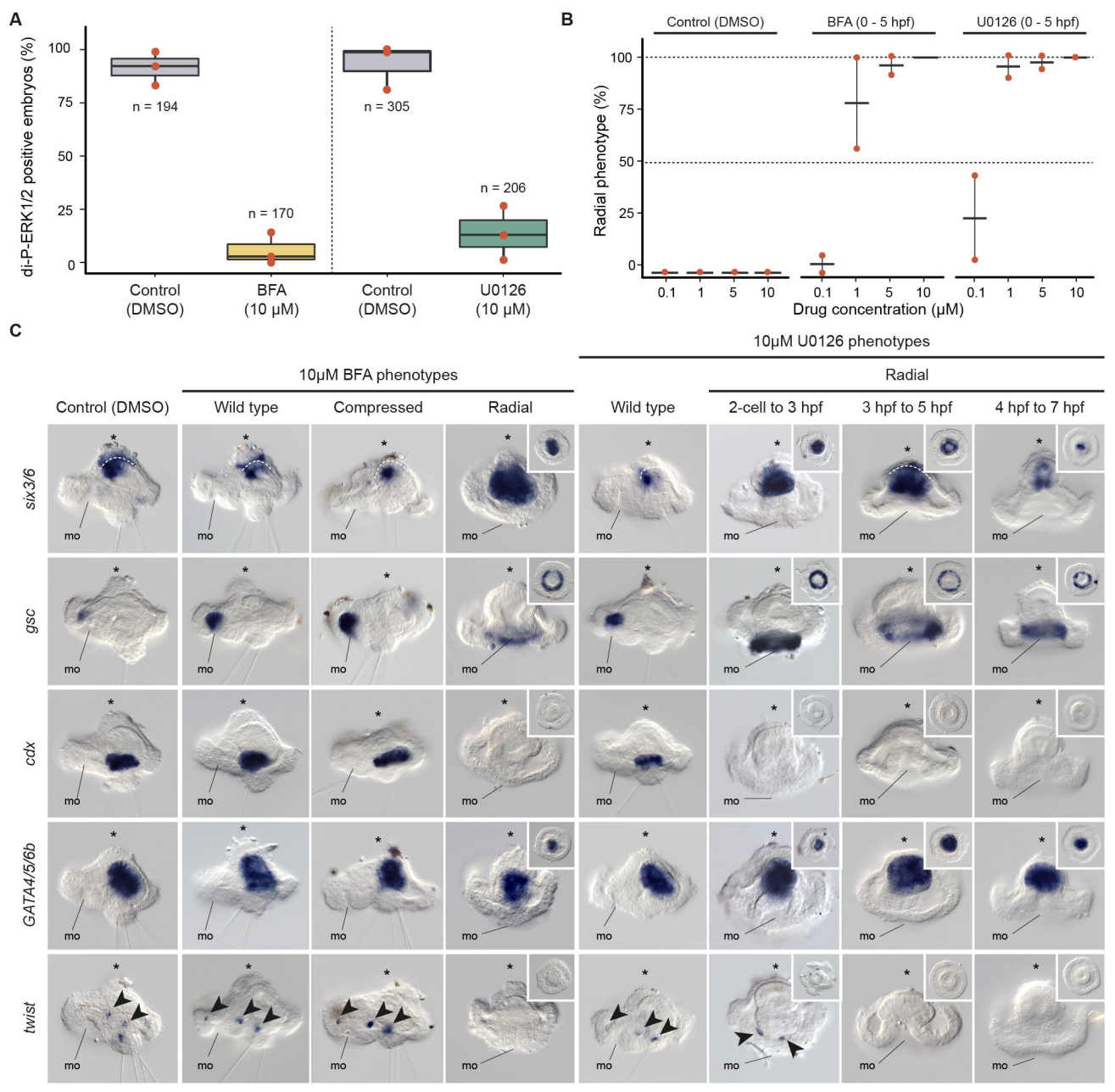
A
di-P-ERK1/2 positive embryos (%)
100
75
50
25
0
n = 194
n = 170
n = 305
n = 206
Control (DMSO)
BFA (10 µM)
Control (DMSO)
U0126 (10 µM)
B
Control (DMSO)
BFA (0 - 5 hpf)
U0126 (0 - 5 hpf)
Radial phenotype (%)
100
75
50
25
0
0.1
1
5
10
Drug concentration (µM)
C
10µM BFA phenotypes
10µM U0126 phenotypes
Radial
Control (DMSO)
Wild type
Compressed
Radial
Wild type
2-cell to 3 hpf
3 hpf to 5 hpf
4 hpf to 7 hpf
six3/6
gsc
cdx
GATA4/5/6b
twist
mo

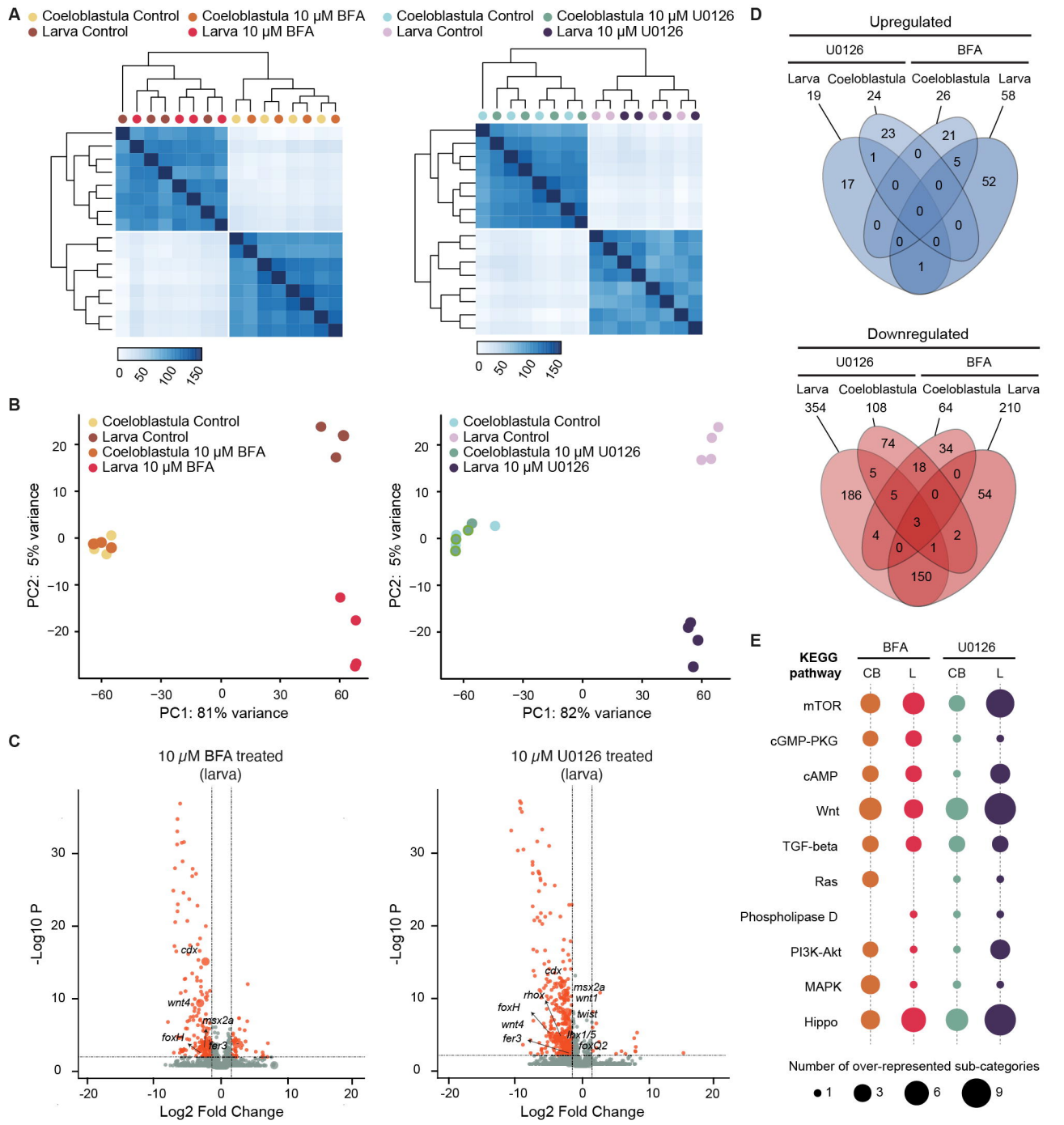
A
Coeloblastula Control
Larva Control
Coeloblastula 10 μM BFA
Larva 10 μM BFA
Coeloblastula Control
Larva Control
Coeloblastula 10 μM U0126
Larva 10 μM U0126
0 50 100 150
B
Coeloblastula Control
Larva Control
Coeloblastula 10 μM BFA
Larva 10 μM BFA
PC2: 5% variance
PC1: 81% variance
Coeloblastula Control
Larva Control
Coeloblastula 10 μM U0126
Larva 10 μM U0126
PC2: 5% variance
PC1: 82% variance
C
10 μM BFA treated (larva)
-Log10 P
Log2 Fold Change
cdx
wnt4
msx2a
foxH
fer3
10 μM U0126 treated (larva)
-Log10 P
Log2 Fold Change
cdx
rhox
msx2a
wnt1
foxH
twist
wnt4
lhx1/5
fer3
foxQ2
D
Upregulated
U0126
BFA
Larva
Coeloblastula
Coeloblastula
Larva
19
24
26
58
23
21
1
0
5
17
0
0
52
0
0
0
0
0
1
Downregulated
U0126
BFA
Larva
Coeloblastula
Coeloblastula
Larva
354
108
64
210
74
34
5
18
0
186
5
0
54
3
4
2
0
1
150
E
KEGG pathway
BFA
U0126
CB
L
CB
L
mTOR
cGMP-PKG
cAMP
Wnt
TGF-beta
Ras
Phospholipase D
PI3K-Akt
MAPK
Hippo
Number of over-represented sub-categories
1
3
6
9

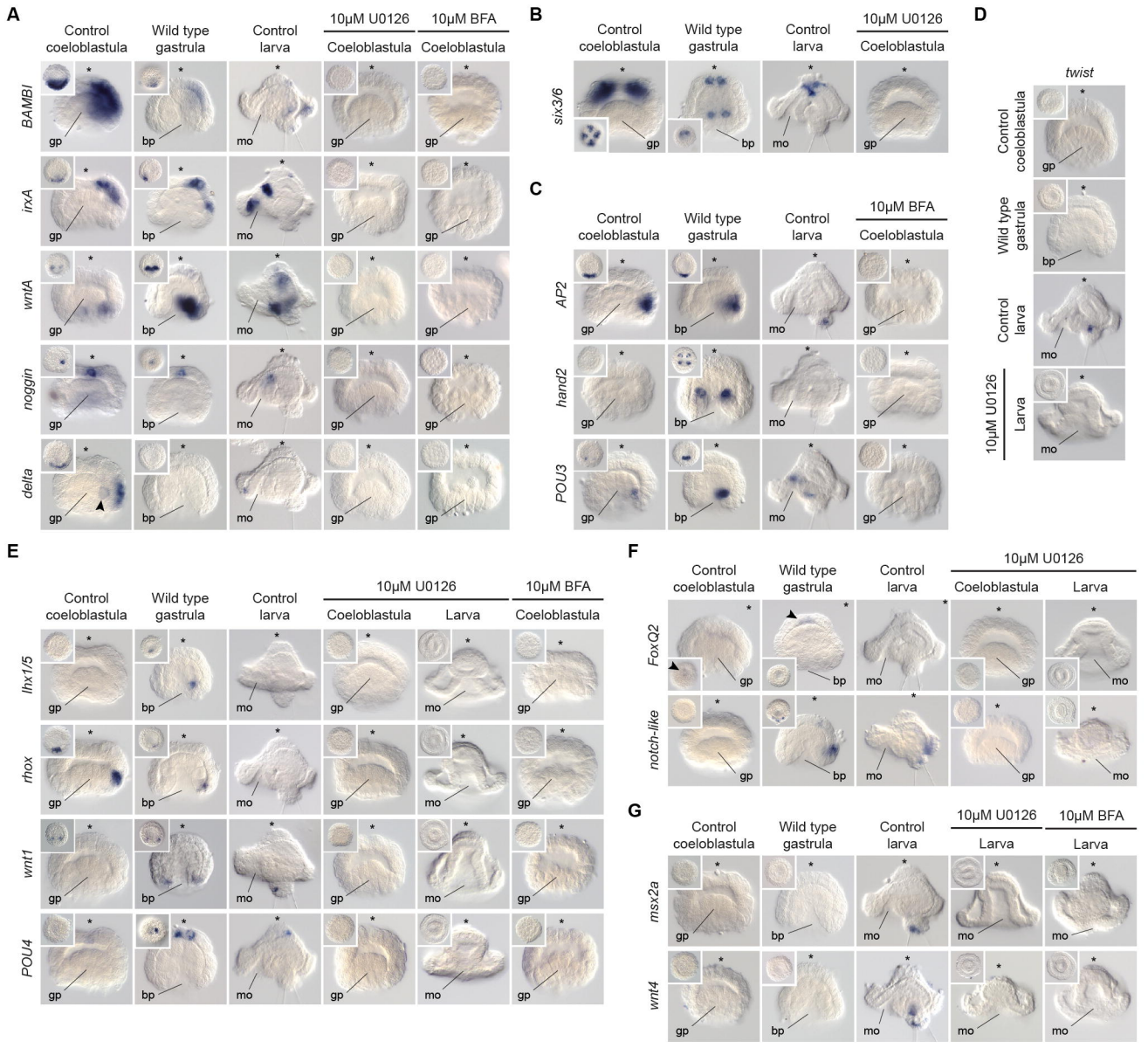
A
Control coeloblastula
Wild type gastrula
Control larva
10μM U0126
10μM BFA
Coeloblastula
Coeloblastula
BAMBI
irxA
wntA
noggin
delta
gp
bp
mo
B
Control coeloblastula
Wild type gastrula
Control larva
10μM U0126
Coeloblastula
six3/6
C
Control coeloblastula
Wild type gastrula
Control larva
10μM BFA
Coeloblastula
AP2
hand2
POU3
D
twist
Control coeloblastula
Wild type gastrula
Control larva
10μM U0126
Larva
E
Control coeloblastula
Wild type gastrula
Control larva
10μM U0126
Coeloblastula
Larva
10μM BFA
Coeloblastula
lhx1/5
rhox
wnt1
POU4
F
Control coeloblastula
Wild type gastrula
Control larva
10μM U0126
Coeloblastula
Larva
FoxQ2
notch-like
G
Control coeloblastula
Wild type gastrula
Control larva
10μM U0126
Larva
10μM BFA
Larva
msx2a
wnt4

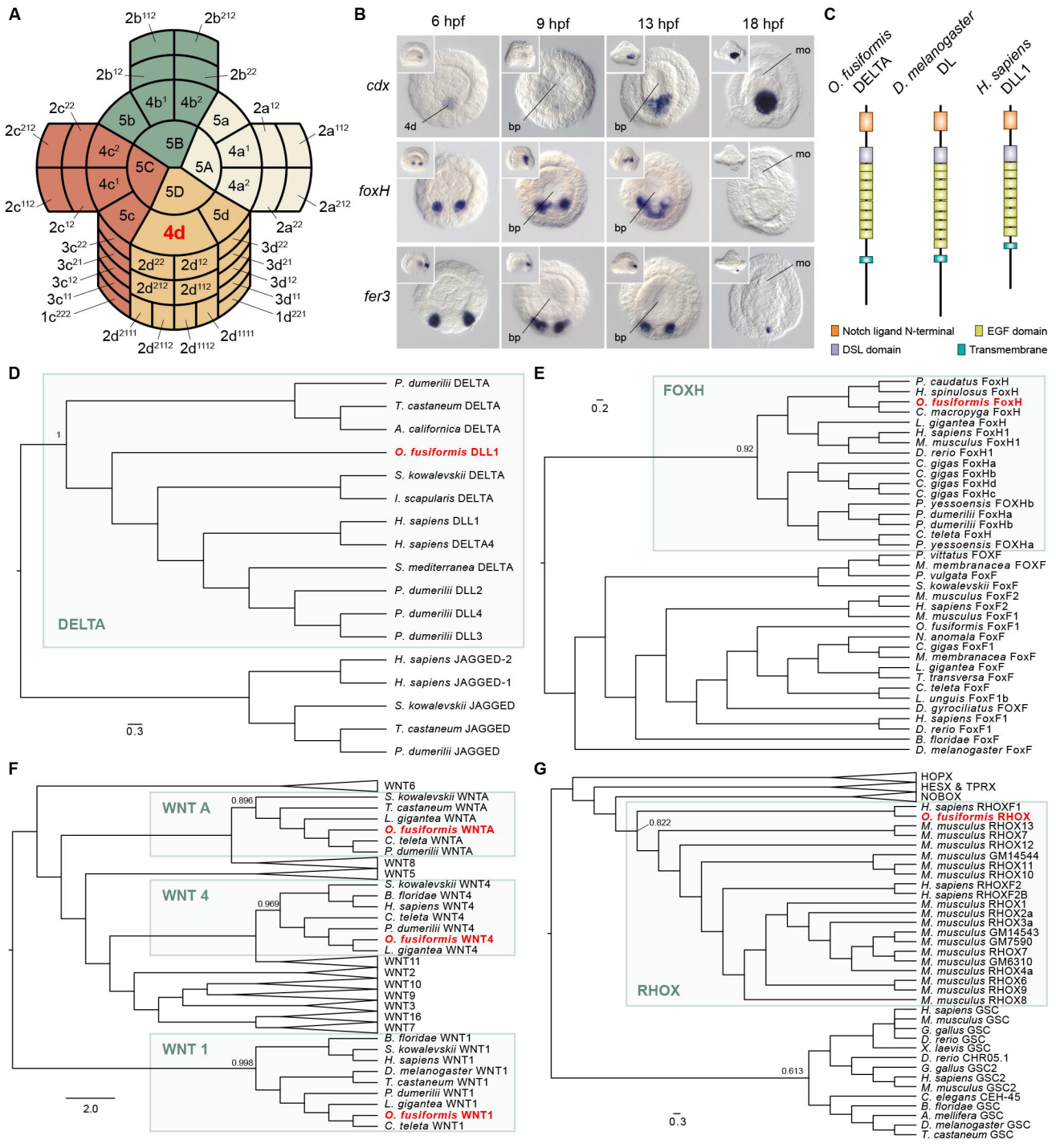
A
2b112
2b212
2b12
2b22
2c22
2a12
2c212
2a112
5b
5a
4b1
4b2
5B
4c2
4a1
5C
5A
4c1
4a2
2c112
2a212
5D
2c12
5c
5d
2a22
4d
3c22
3d22
3c21
3d21
2d22
2d12
3c12
2d212
2d112
3d12
3c11
3d11
1c222
1d221
2d2111
2d1111
2d2112
2d1112
B
6 hpf
9 hpf
13 hpf
18 hpf
cdx
foxH
fer3
4d
bp
mo
C
O. fusiformis DELTA
D. melanogaster DL
H. sapiens DLL1
Notch ligand N-terminal
EGF domain
DSL domain
Transmembrane
D
DELTA
P. dumerilii DELTA
T. castaneum DELTA
A. californica DELTA
O. fusiformis DLL1
S. kowalevskii DELTA
I. scapularis DELTA
H. sapiens DLL1
H. sapiens DELTA4
S. mediterranea DELTA
P. dumerilii DLL2
P. dumerilii DLL4
P. dumerilii DLL3
H. sapiens JAGGED-2
H. sapiens JAGGED-1
S. kowalevskii JAGGED
T. castaneum JAGGED
P. dumerilii JAGGED
1
0.3
E
FOXH
0.2
0.92
P. caudatus FoxH
H. spinulosus FoxH
O. fusiformis FoxH
C. macropyga FoxH
L. gigantea FoxH
H. sapiens FoxH1
M. musculus FoxH1
D. rerio FoxH1
C. gigas FoxHa
C. gigas FoxHb
C. gigas FoxHd
C. gigas FoxHc
P. yessoensis FOXHb
P. dumerilii FoxHa
P. dumerilii FoxHb
C. teleta FoxH
P. yessoensis FOXHa
P. vittatus FOXF
M. membranacea FOXF
P. vulgata FoxF
S. kowalevskii FoxF
M. musculus FoxF2
H. sapiens FoxF2
M. musculus FoxF1
O. fusiformis FoxF1
N. anomala FoxF
C. gigas FoxF1
M. membranacea FoxF
L. gigantea FoxF
T. transversa FoxF
C. teleta FoxF
L. unguis FoxF1b
D. gyrociliatus FOXF
H. sapiens FoxF1
D. rerio FoxF1
B. floridae FoxF
D. melanogaster FoxF
F
WNT A
0.896
WNT6
S. kowalevskii WNTA
T. castaneum WNTA
L. gigantea WNTA
O. fusiformis WNTA
C. teleta WNTA
P. dumerilii WNTA
WNT8
WNT5
WNT 4
0.969
S. kowalevskii WNT4
B. floridae WNT4
H. sapiens WNT4
C. teleta WNT4
P. dumerilii WNT4
O. fusiformis WNT4
L. gigantea WNT4
WNT11
WNT2
WNT10
WNT9
WNT3
WNT16
WNT7
WNT 1
0.998
B. floridae WNT1
S. kowalevskii WNT1
H. sapiens WNT1
D. melanogaster WNT1
T. castaneum WNT1
P. dumerilii WNT1
L. gigantea WNT1
O. fusiformis WNT1
C. teleta WNT1
2.0
G
HOPX
HESX & TPRX
NOBOX
0.822
H. sapiens RHOXF1
O. fusiformis RHOX
M. musculus RHOX13
M. musculus RHOX7
M. musculus RHOX12
M. musculus GM14544
M. musculus RHOX11
M. musculus RHOX10
H. sapiens RHOXF2
H. sapiens RHOXF2B
M. musculus RHOX1
M. musculus RHOX2a
M. musculus RHOX3a
M. musculus GM14543
M. musculus GM7590
M. musculus RHOX7
M. musculus GM6310
M. musculus RHOX4a
M. musculus RHOX6
M. musculus RHOX9
M. musculus RHOX8
RHOX
H. sapiens GSC
M. musculus GSC
G. gallus GSC
D. rerio GSC
X. laevis GSC
D. rerio CHR05.1
G. gallus GSC2
H. sapiens GSC2
M. musculus GSC2
C. elegans CEH-45
B. floridae GSC
A. mellifera GSC
D. melanogaster GSC
T. castaneum GSC
0.613
0.3

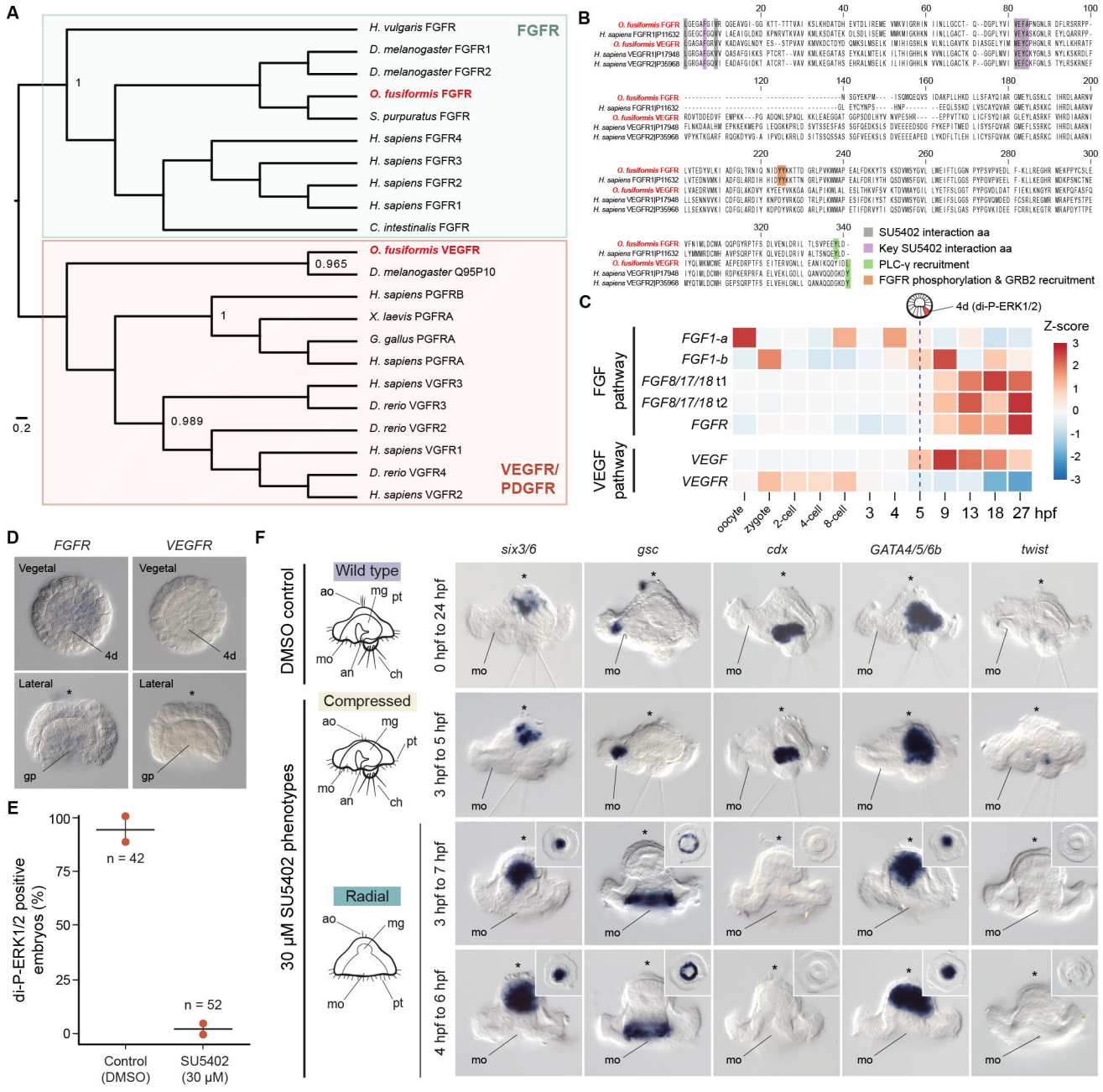
A
FGFR
H. vulgaris FGFR
D. melanogaster FGFR1
D. melanogaster FGFR2
O. fusiformis FGFR
S. purpuratus FGFR
H. sapiens FGFR4
H. sapiens FGFR3
H. sapiens FGFR2
H. sapiens FGFR1
C. intestinalis FGFR
O. fusiformis VEGFR
D. melanogaster Q95P10
H. sapiens PGFRB
X. laevis PGFRA
G. gallus PGFRA
H. sapiens PGFRA
H. sapiens VGFR3
D. rerio VGFR3
D. rerio VGFR2
H. sapiens VGFR1
D. rerio VGFR4
H. sapiens VGFR2
VEGFR/ PDGFR
1
0.965
1
0.989
0.2
B
O. fusiformis FGFR
H. sapiens FGFR1|P11632
O. fusiformis VEGFR
H. sapiens VEGFR1|P17948
H. sapiens VEGFR2|P35968
SU5402 interaction aa
Key SU5402 interaction aa
PLC-γ recruitment
FGFR phosphorylation & GRB2 recruitment
C
4d (di-P-ERK1/2)
Z-score
FGF pathway
FGF1-a
FGF1-b
FGF8/17/18 t1
FGF8/17/18 t2
FGFR
VEGF pathway
VEGF
VEGFR
oocyte
zygote
2-cell
4-cell
8-cell
3
4
5
9
13
18
27 hpf
D
FGFR
VEGFR
Vegetal
4d
Lateral
gp
E
di-P-ERK1/2 positive embryos (%)
n = 42
n = 52
Control (DMSO)
SU5402 (30 μM)
F
DMSO control
30 μM SU5402 phenotypes
Wild type
Compressed
Radial
ao
mg
pt
mo
an
ch
six3/6
gsc
cdx
GATA4/5/6b
twist
0 hpf to 24 hpf
3 hpf to 5 hpf
3 hpf to 7 hpf
4 hpf to 6 hpf